

Application of QD-MOF composites for photocatalysis: Energy production and environmental remediation

Ting Wu ^{a,1}, Xiaojuan Liu ^{b,1}, Yang Liu ^{a,1}, Min Cheng ^{a,1}, Zhifeng Liu ^{a,*}, Guangming Zeng ^{a,*}, Binbin Shao ^a, Qinghua Liang ^a, Wei Zhang ^a, Qingyun He ^a, Wei Zhang ^b

^a College of Environmental Science and Engineering, Hunan University and Key Laboratory of Environmental Biology and Pollution Control (Hunan University), Ministry of Education, Changsha 410082, P.R. China

^b The First Affiliated Hospital of Hunan University of Chinese Medicine, Changsha 410007, P.R. China.

* Corresponding authors at:

^a College of Environmental Science and Engineering, Hunan University and Key Laboratory of Environmental Biology and Pollution Control (Hunan University), Ministry of Education, Changsha 410082, P.R. China

E-mail: zhifengliu@hnu.edu.cn (Z. Liu)

E-mail: zgming@hnu.edu.cn (G. Zeng)

¹ The authors contribute equally to this paper.

Abstract

Photocatalysis is an efficient technology for energy production and environmental remediation. The composites of metal organic frameworks (MOFs) combined with quantum dots (QDs) allow high photocatalytic ability. Recently, these composites have been applied increasingly in the fields of energy production and environmental remediation. Even so, QD-MOF composites still have some shortcomings in the field of photocatalysis. In this review, the synthesis methods and structures as well as the applications of QD-MOF composites in water splitting for hydrogen production, carbon dioxide (CO₂) reduction to produce methane (CH₄), organic dye degradation, Cr(VI) reduction, and nitric oxide (NO) oxidation are discussed. The mechanisms of these processes are also described in detail. Finally, new insights into the future development and challenges of the composite are proposed to advance further development of the research area.

Keywords: Metal-organic frameworks, Quantum dots, Photocatalysis, Energy production, Environmental remediation.

Content

1. Introduction.....	4
2. Structure and properties of QDs and MOFs and QD-MOF	6
2.1. Structure and properties of QDs.....	6
2.2. Structure and properties of MOFs.....	8
2.3. Structure and properties of QD-MOF composites	10
3. Synthesis methods of QD-MOF composites	12
3.1 Ship-in-a-bottle	13
3.2 Bottle-around-the-ship	15
3.3 Photochemical deposition	16
3.4 Direct surface functionalization	17
3.5 Other synthesis methods	17
4. QD-MOF composites for photocatalysis.....	19
4.1 Energy production	19
4.1.1 Hydrogen production by water splitting.....	19
4.1.2 Carbon dioxide reduction to produce methane.....	25
4.2 Environmental modification.....	28
4.2.1 Organic dye degradation.	28
4.2.2 Cr (VI) reduction	30
4.2.3 Nitric oxide oxidation	32
5. Summary and Perspective.....	34
Acknowledgements	39
References.....	39

1. Introduction

Environmental pollution and resource depletion have become the two major problems to humans [1-3]. In view of the abundant and sustainable solar energy, photocatalysis has attracted worldwide attention in environmental remediation and energy production in the past few decades [4-7]. Therefore, a large number of photocatalysts have been fabricated and used in the fields of environmental remediation and energy production, and they have been rapidly developed [8-12]. However, the disadvantages of single-phase photocatalysts, such as easy aggregation in solution, poor tenability, wide band gap, slow photogenic electron transmission, high photogenic carrier recombination rate, and only responding to ultraviolet light and so on, leading to low photoenergy utilization efficiency and low photocatalytic capacity [13, 14]. Hence novel photocatalysts are expected to be explored.

Combining different functional materials to prepare composite photocatalyst is an effective way to conquer the disadvantages of single-phase photocatalyst [15-17]. Many composite photocatalysts have been prepared, such as semiconductor nanoparticles combined with semiconductor nanoparticles [18-20], metal nanoparticles combined with semiconductor nanoparticles [21, 22], conjugated polymers combined with nanocrystal composites [23] and so on. These binary and even multicomponent composites exhibit higher photocatalytic performance than single-phase materials.

With the appearance of various metal organic framework (MOF) materials (MIL, UIO, ZIF, PCN, CPL, HUST, IRMOF etc.), which possess ordered porous structure

and large specific surface area as well as abundant active sites have attracted attention of researchers [24, 25]. The unique structure of MOFs makes it an ideal material to combine with other functional materials [26, 27]. As a special type of semiconductor material, quantum dots (QDs) have strong light capture ability and extinction coefficient, which can effectively promote the transmission of photogenerated electrons and inhibit the recombination of electron-hole pairs [13]. Although MOFs and QDs have the above excellent properties, the low light absorption ability and instability of MOFs and the rapid photogenerated charge recombination rate and easy agglomeration of QDs are the main factors limiting their use as photocatalysts individually [28, 29]. Excitingly, MOFs with porous structure and large specific surface area provide a dispersive place for QDs to prevent them from aggregating and ensure that QDs effectively receive light irradiation. In turn, QDs improve the photoelectric performance and light absorption capacity of MOFs [30]. The close interface and matched band gap between QDs and MOFs accelerate the separation of photogenerated charges, effectively inhibit the recombination of photogenerated electrons and holes, and thus enhance the photocatalytic performance. Hence the studies of QD-MOF composites have gradually emerged and they show a bright application prospect in the field of photocatalysis. In the past few years, the synthesis and application of QD-MOF composites have made new breakthroughs, but the development of them is not very mature, and the application is still limited. Besides, the review of QD-MOF composites in photocatalysis for energy production and environmental remediation and the related mechanisms have not been reported. In

order to further understand the characteristics and properties of the composites in the photocatalytic reaction process, it is necessary to have a review for these composites in the field of photocatalysis.

Herein, we concentrate on the synthesis methods and structures of QD-MOF composites and their application in energy production and environmental remediation. According to the current research status, it mainly including water splitting for hydrogen production, carbon dioxide (CO₂) reduction to produce methane (CH₄), organic dye degradation, Cr(VI) reduction, and nitric oxide (NO) oxidation. Particularly, the photocatalytic mechanisms of these composites were described in detail, and the challenges and future development trends of them were prospected.

2. Structures and properties of QDs and MOFs and QD-MOF composites

2.1. Structure and properties of QDs

QDs are a series of fluorescent semiconductor nanoparticles with size 1 to 10 nm, containing approximately 200 to 10,000 atoms [31]. Usually, the QDs are core (e.g. TiO₂, CdS, InP, GaAs, GaN)-shell (e.g. ZnS, ZnO, CdS, PbS, CdSe) structure. [13] (Fig. 1). Due to the large specific surface area and quantum confinement effect (excitons are constrained in three dimensions and the continuous energy levels become discrete), QDs possess specific physicochemical properties, including long lifetimes, low photobleaching, high luminescent quantum yields and extinction coefficients, wide absorption spectra and narrow emission spectra [32]. The band gap of QDs increases with the decrease of particle size, so the absorption spectrum of QDs can be changed by adjusting their size [13]. Besides, small QDs exhibit faster electron

transfer rates and higher photocatalytic performance due to their higher specific surface area and more active sites than large QDs [33]. Amazingly, the photocatalytic properties and photoluminescence of QDs can be improved by doping metal ions [13]. For example, Ma et al. [34] co-doped Co and K ions into CdSe QDs. The doped CdSe QDs not only showed better photostability under visible light, but also appeared higher photocatalytic ability for tetracycline hydrochloride. Mojtaba et al. [35] doped Fe^{3+} in the ZnS QDs, resulting in a decrease in the particle size of QDs, thus a blue shift was appeared in the absorption spectrum. And the Fe^{3+} doped ZnS QDs showed better decolorization rate and photodegradation ability for methyl violet (MV) under ultraviolet light. Besides, through the chemical attachment or intermolecular force, the monolayer organic molecules (e.g. capping agents, ligands or linkers) are combined with the surface atoms of nanocrystals to maintain the stability of QDs [36-38]. A certain number of ligands and capping agents, including oleic acid [39], chitosan [40], 2-mercaptoethanol [41-43], thioglycolic acid (TGA) [44], 3-mercaptopropionic acid (3MPA) [45], thiolactic acid (TLG) and triethoxysilane (APTES) [13] and so on have been used as stability layer effectively to change the toxicity, particle size, morphology, physicochemical properties and optical characteristics of QDs. Meanwhile, the luminescent quantum yields are more than pure QDs [46]. Additionally, functionalization of the QDs surface not only enhance their stability but also keep them from aggregating [47]. For instance, Ma et al. [48] synthesized high hydrosoluble CdTe QDs by coating with 3MPA. The capped CdTe QDs showed high stability and quantum yield (82%). Moreover, these QDs still showed strong

fluorescence emission ability in red to near-infrared region. Mansur et al. [49] functionalized ZnS QDs with chitosan and the abundant hydroxyl, amino and acetamide carboxyl groups on chitosan combined with ZnS QDs to form conjugated polymers. The functionalized QDs displayed high long-term stability and excellent photodegradability for methylene blue (MB). Furthermore, a proper shell and oxide overcoating design can protect QDs from water damage [50]. For example, Fu et al. synthesized CdSe@ZnS/ZnS QDs with thick shell. The obtained QDs still maintained excellent stability in the condition of 85% relative humidity [51]. Zhang et al. coated the CsPbBr₃ surface with SiO₂ shell, significantly improving the stability against water [52]. In order to promote the water-dispersible, QDs are encapsulated in amphiphilic oligomers [53], and surfactants [54], which play a role to cover hydrophobic surface of QDs and result in well dispersible in water [31]. Expectedly, with the above-mentioned advantages, QDs have been widely applied in many fields, such as drug delivery [55, 56], bioimaging [57, 58], biosensing [59, 60], solar cells [61, 62], electrochemiluminescence [63, 64], photoelectrochemical sensors [65, 66] as well as photocatalysis [42, 43, 67].

2.2. Structure and properties of MOFs

MOFs are a series of promising microporous crystalline materials, which are known as porous coordination polymers (PCPs) [68, 69]. They are composed of metal nodes or clusters and organic ligands [70, 71]. The structure and properties of MOFs can be designed by transforming the species of metal clusters and ligands [72, 73]. For example, ZIF-8 and the ZIF-11 have the same ZnN₄ tetrahedral metal center, but

with different organic linkers, that are 2-methylimidazolate and benzimidazolate, respectively (Fig. 2a). Thus ZIF-8 and ZIF-11 show different porosity (11.6 Å and 14.6 Å in diameter) and specific surface area ($1947 \text{ m}^2 \text{ g}^{-1}$ and $1676 \text{ m}^2 \text{ g}^{-1}$) as well as physicochemical properties [74, 75]. Besides, ZIF-67 with CoN_4 tetrahedral metal centers and 2-methylimidazolate organic linkers behaves different stability and catalytic activity from ZIF-8 due to the difference of electrostatic force between Zn^{2+} and Co^{2+} . Another typical example is the Zr-based MOFs UiO-66, UiO-67, and UiO-68, which behave different properties by changing the length of the organic linkers. With the increase of organic linker length, the stability of MOFs are decreased [76] (Fig. 2b). Moreover, functional materials such as enzymes [77], metal nanoparticles [78, 79], metalloporphyrins [80] and so on can be encapsulated in the pores of MOFs to regulate their functions [81, 82]. Meanwhile, MOFs are remarkable scaffolds due to the ordered channels and ultrahigh surface area which allow high mass loading, preventing nanoparticles from aggregation that damages material performance [83]. For the above reasons, MOFs have been used in many fields such as luminescence [84, 85], energy storage [86, 87] and conversion [87, 88], gas separation and adsorption [89, 90], chemical sensing [91, 92], biomedicine [93, 94], and proton conduction [95-97].

In addition, MOFs are supposed to be promising candidates for photocatalyst [98]. In this case, stability and broad absorption spectrum of MOFs are required. Many factors can affect the stability of MOFs, such as the type and size of metal ions and organic linkers, hydrophobicity of the pore surface, coordination geometry of

metal-ligands, particle size of MOFs, and operating environment, etc. [72]. Generally, the MOFs formed by high-valent metal ions exhibit higher stability. The main reasons may be that the high-valent metal ions can not only form strong metal-ligand coordination bonds, but also form high steric hindrance with linkers [99, 100]. As for the composites of MOFs, designing hydrophobic surface and/or post-synthetic modification are effective methods to improve their stability [101-104].

In order to increase the light respond ability of MOFs, the commonly used strategies are to modify organic connectors by functional groups, change the metal centers, and combine narrow-band gap semiconductors to construct heterogeneous structures [105]. Among them, construction of heterojunctions is the most effective strategy. Through these methods, a large number of MOFs with different physicochemical properties can be synthesized successfully. Therefore, MOFs would play an important part in the development of photocatalysis [106].

2.3. Structure and properties of QD-MOF composites

Due to the different matching degree between QD size and MOF pore size and different assembly methods, the morphology of QD-MOF composites can be divided into three types. The first is QDs within the pore of MOF, which the QDs are almost encapsulated in the frameworks of MOFs (Fig. 3a). In this structure, the growth and alignment of the QDs are limited, and QDs can be immobilized in the MOF matrix in an orderly manner without agglomeration. Wang et al. [107] synthesized CdTe@ZIF-8 with core-shell structure that numerous CdTe QDs were contained in the ZIF-8 orderly and dispersedly (Fig. 3b). Biswal et al. [108] encapsulated GQDs

(Graphene quantum dots) into ZIF-8 through interaction between zinc ion of ZIF-8 and carboxylic acid of GQDs (Fig. 3c). The special Zinc-carboxyl bonds promoted the combination between GQDs and ZIF-8, and inhibited the aggregation of GQDs in the ZIF-8. In the second structure, some QDs are embedded in the MOF matrix, while others are exposed on the surface of the MOF (Fig. 3d). The possible reason is that the size of some QDs is larger than the pore size of MOFs, thus QDs cannot all enter into the interior of MOFs through the pores, resulting in some QDs being exposed on the surface of MOFs. In addition, when the number of QDs is more than the pore of MOFs, excessive QDs will also deposit on the MOF surface. He et al. [109] embedded CdS QDs into MIL-101, and the excessive CdS QDs were agglomerated on the MIL-101 surface (Fig. 3e). Gan et al. [110] synthesized UiO-66 embedded with CdSe. The HRTEM images show that CdSe QDs were grown both inside and outside of the MOFs, and the size of CdSe QDs on the outer surface were larger than those inside the MOFs (Fig. 3f). The third structure shows that QDs are all anchored on the outer surface of MOFs. In this case, the growth of QDs is not restricted, which is likely to lead to an aggregation on the MOFs surface, resulting in the inhomogeneity of composite particles [83] (Fig. 3g). Li et al. [111] synthesized the core-shell structure with $\text{Cu}_3(\text{BTC})_2$ as the core and TiO_2 as the shell. The shell with 210 nm thick enclosed the core to form a rough and porous surface on $\text{Cu}_3(\text{BTC})_2$ (Fig. 3h). Xu et al. [112] immobilized ZnO QDs of 10nm on ZUM and the pore size of ZUM had not been changed. Therefore, it can be speculated that ZnO QDs did not enter into the ZUM matrix rather agglomerated on the surface. The TEM images also confirmed

the agglomeration of ZnO QDs (Fig. 3i).

Combined QDs with MOFs effectively overcome the shortcomings of the QDs and MOFs. Using QDs alone tend to agglomerate in an aqueous solution, resulting in a weakening of light absorption [113]. Besides, photogenerated charges in QDs are easily recombined, resulting in low photocatalytic efficiency [114]. Furthermore, the poor stability and light absorption ability resulting in low photocatalytic performance of MOFs [115]. As for the QD-MOF materials, because of the large specific surface area and orderly pores of MOFs, it provides a favorable space for loading QDs and preventing QDs aggregating. Meanwhile, QDs improve the physicochemical properties of MOFs [116]. The intimate heterostructure or interfacial interaction between QDs and MOFs accelerate electron transport and effectively inhibit photogenerated charges recombination [117]. Therefore, the combination of QDs and MOFs lead to good dispersion, high stability and photocatalytic activity [118]. In the QD-MOF composites, the addition of QDs will occupy the pores of the MOFs, so that, compared with the pure MOF materials, the porosity and specific surface area of the QD-MOF composites are reduced. Nevertheless, due to the coordination between QDs and MOFs, the photocatalytic performance is still enhanced. However, once QDs are overloaded, the pores of MOFs are blocked or even covered. At this time, the photocatalytic activity of QD-MOF composites is reduced with the decrease of porosity and specific surface area [109, 119, 120].

3. Synthesis methods of QD-MOF composites

There are four main synthesis methods have been reported to synthesize

QD-MOF composites. Two well-constructed methods are “ship-in-a-bottle” and “bottle-around-the-ship” which have been exploited to encapsulate QDs in the MOF matrix. Another two methods are “photodeposition” and “direct surface functionalization”, that tend to immobilize QDs on the surface of MOFs [118]. Besides, some emerging methods to combine QDs with MOF matrix have been reported. In this part, these methods are described in detail.

3.1 Ship-in-a-bottle

The “ship-in-a-bottle” method needs to infiltrate or deposit QDs or QD precursors through the preformed MOF matrix. This assembly process prioritizes the synthesis of the MOF matrix, and then the synthesis of QDs in the MOF (Fig. 4a). Depending on the synthesis conditions, the “ship-in-a-bottle” method for the synthesis of QD-MOF composites can be sorted to three categories, including “chemical vapor infiltration”, “solution infiltration” and “double solution method”.

The “chemical vapor infiltration” employs a vacuumed Schlenk tube with two heating zone. One or more QD precursors are put in the former heating area of the vacuumed Schlenk tube. Meanwhile, the designated MOFs are put in the downstream heating area. An appropriate temperature is heated to induce a sublimation of QD precursors and further introduce the precursor vapor infiltrate into MOF matrix. In this process, the tube needs to be filled with carrier gas and continuously pump to bring the steam from the precursors into the MOFs. QD precursors deposited into the MOFs instantaneously when the hot precursor vapor gets in touch with relatively cold MOF substrate. After deposition, precursor-decorated substrate is heated and reducing

gas is induced to convert QD precursors to QDs, and formed QD-MOF (Fig. 4b). Through this method, volatile organic metal molecules $[\text{Zn}(\text{C}_2\text{H}_5)_2]$ and $[(\text{CH}_3)_3\text{NGaH}_3]$ were permeated into ZIF-8 respectively and further transform into ZnO@ZIF-8 and GaN@ZIF-8 composites by high temperature annealing process [121, 122]. Compared to “chemical vapor infiltration”, the “solution infiltration” is a moderate technology that only requires the immersion of MOF into the solution containing QD precursors. After immersion, the MOF is leached and washed to remove redundant salts or uncontrolled QD precursors. Finally, the QD precursors are grown to QDs, forming target QD-MOF (Fig. 4c). Gao et al.[123] immersed ZIF-8 into the SnO_2 QD precursors solution and then added hydrogen peroxide to realize the formation of $\text{SnO}_2\text{@ZIF-8}$ composite. Chen et al. [124] synthesized perovskite QDs encapsulated HKUST-1 through two steps, including adding HKUST-1 to PbI_2 solution to obtain $\text{PbI}_2\text{@HKUST-1}$ and adding $\text{CH}_3\text{NH}_3\text{X}$ ($\text{X} = \text{Cl}, \text{Br}, \text{I}$) ethanol solution into as-prepared $\text{PbI}_2\text{@HKUST-1}$ solution to form $\text{CH}_3\text{NH}_3\text{PbI}_2\text{X@HKUST-1}$. Zhang et al. [125] mixed UiO-67 with CsPbX_3 QD precursors solution through thermal injection to obtain $\text{CsPbX}_3\text{@UiO-67}$ at high temperature condition. Accordingly, in solution infiltration process, water-stable MOFs and QDs are required. However, one drawback of this method is that it is difficult to avoid the deposition of QDs on the outer surface of the MOFs. Therefore, this method was optimized to “double solution method” (Fig. 4d). In this method, the QD precursors with less than the capacity of MOF pores enter the hydrophilic pores of the MOFs by capillary force and hydrophilic interaction, thus minimizing the deposition of QDs on the MOF

surface. Besides, the pores of MOFs as the confine reactors to control the size of QDs, preventing QDs from aggregating [68, 126]. Meng and co-workers [119] co-infiltrated slight glucose and CdS QD precursor solution into the hydrophilic pores of activated MIL-101 by double solution method to formed G/CdS@MIL-101 (G represented graphene). After that, G/CdS@MIL-101 was calcined at a high temperature of 200 °C to obtain the final product CD/CdS@MIL-101.

As above description, harsh reaction conditions are referred by using “ship-in-a-bottle” to synthesize QD-MOF, such as high temperature and/or redox condition, which may destroy the structure of MOFs. Thus, particular stable MOFs is required. Nevertheless, the most significant advantage of this approach is that , the formation of conformal MOF layers around QDs could be achieved, which is considered as a remarkable and challenging process in this strategy [83, 118].

3.2 Bottle-around-the-ship

The “bottle-around-the-ship” is the method of assembling the precursors of MOF around QDs and then synthesizing QD-MOF (Fig. 5a). In this synthesis strategy, QDs are firstly prepared and dispersed in solvent containing stabilizer such as surfactant, which prevents QDs from agglomeration. Subsequently, MOF building blocks are put in the solvent and launch MOF growth around the QDs. In this assemble process, organic links bond to capping agents on the surface of QDs by divalent bonds [83]. Wang et al. [107] capped polyvinyl pyrrolidone (PVP) agent on the surface of CdTe QDs and the capped CdTe QDs not only guaranteed the stability and dispersion but also promoted the growth of ZIF-8 on the surface of CdTe QDs and formed intimate

heterogeneous structure between them. Kaur et al. [127] added cysteamine capped CdTe QDs into the Eu-MOF precursors solution to synthesize CdTe/Eu-MOF composite. The interaction between the amino groups on the surface of the CdTe QDs and the carboxyl groups of Eu-MOF achieved CdTe QDs distributed in the Eu-MOF matrix in an orderly manner. By using this method, QDs are encapsulated in the matrix basically instead of the pore space of MOFs and therefore ensures the distribution of nanoparticles throughout the MOF matrix. Additionally, this strategy not only avoids the diffusion resistance of nanoparticles to infiltrate into the matrix of MOFs, allowing the QDs deposited into MOF matrix easily, but also effectively reduces the amount of QDs deposited on the outer surface of MOFs [128]. Moreover, since the nanoparticles can be pre-formed before assembling the frameworks, the size and shape of QDs can be adjusted for application [118].

3.3 Photochemical deposition

Different from the methods of “ship-in-the-bottle” and “bottle-around-the-ship”, which QDs were contained in the MOFs, “photochemical deposition” method is to deposit QDs on the surface of MOFs (Fig. 5b). Synthesis of QD-MOF composites by this strategy need two important procedures including in situ formation and deposition of QDs on the surface of MOFs. In the process of QDs deposition, an appropriate photoreduction potential is needed to transform the QD precursors to QDs, insuring the synthesis of QD-MOF composites successfully. Lin et al. [129] dissolved UiO-66 into CdS QDs precursor solution and obtained the composite of UiO-66 modified CdS QDs through light radiation. The resulting composite showed that the CdS QDs were

uniformly distributed on the surface of UiO-66. In the same way, Yuan's group [130] synthesized the composites of MIL-125 (Ti) deposited by CdS, CuS and Ag₂S QDs by ultraviolet radiation. The TEM images showed that a large number of QDs were highly dispersed on the MOF surface.

3.4 Direct surface functionalization

Direct surface functionalization is the strategy to immobilize QDs on the surface of MOFs by appropriate ligands (Fig. 5c). The surface ligands of QDs can be changed by covering different capping groups. Then QDs directly contact with MOFs by coordinative interaction between capping groups and metal ions of MOFs. Jin et al. [131] synthesized amino functionalized CdSe/ZnS core-shell QDs and used to sensitize porphyrin-based MOF. The functionalized QDs were tightly attached on the surface of the MOFs by binding the amino groups of QDs to the zinc points of the porphyrin-based MOF. In this synthesis method, MOFs and QDs are pre-formed before their assembling, which is different from the above three methods. The advantage of this synthesis method is that the shape and size of QDs and the morphology of MOFs can be controlled expediently [118].

3.5 Other synthesis methods

In addition to the above four approaches, there are some uncommon and emerging methods for synthesizing QD-MOF composites, such as, "physical mixing" [132-137], "electrochemical deposition" [138, 139] etc. It is worth mentioning that the "physical mixing" method is more convenient and it can be divided into two modes.

One is to combine QDs and MOFs by physical initiative adsorption, the other is by ultrasonic hybridization. Sammi et al. [133] synthesized the composite of Eu-capped GQDs modified ZIF-8 through physical mixing and the Eu-capped GQDs were attached to the ZIF-8 through physical adsorption. In the same way, Ren et al. [134] embedded the CsPbX₃ QDs into the mesoporous MOF-5 to obtain CsPbX₃ QDs/MOF-5 composite, which not only effectively increased stability of the CsPbX₃ QDs but also retained the optical properties of them. Slightly differently, Xin et al. [136] mixed 2D-MoS₂ QDs solution and MOF-545-Zn solution in an equal volume and conducted ultrasound treatment for half an hour to obtain MOF-545-Zn@MQDs. Wan et al. [137] synthesized CsPbBr₃ QDs/UiO-66(NH₂) nanostructure by mixing the UiO-66(NH₂) powder with CsPbBr₃ QDs solution through ultrasonic hybridization, and the CsPbBr₃ QDs were attached to UiO-66(NH₂) surface and formed a close contact interface between them. As for electrochemical deposition, the QDs are dispersed in an electrolyte and deposited on the surface of MOFs under the action of electric current. Zhen et al. [138] deposited the N-GQDs on the surface of the carbonized MOF-5 (c-MOF-5) by a two-electrode system that c-MOF-5 as the working electrode and Pt as the counter electrode as well as the N-GQD suspension as the electrolyte to obtain N-GQDs/c-MOF-5 composite. In addition, the same group also deposited N-GQDs onto the carbonized ZIF-8 surface in the same way [139]. Generally, these emerging methods tend to construct QDs on the surface of MOFs, and both QDs and MOFs are pre-synthesized before assembling.

In the above methods of synthesizing QD-MOF composites, the strategies of

encapsulating QDs within MOF matrixes are better than coating of MOF crystals with QDs. Encapsulating QDs into MOF matrixes promotes QDs contact with active units of MOFs to form more heterojunctions, which accelerates the separation of photogenerated charges [140]. In addition, encapsulating QDs inside MOFs not only prevents QDs from masking MOFs, but also prevents QDs from agglomeration, thus promoting QDs to receive more light radiation. Furthermore, the stability of QDs will be improved after encapsulating by MOFs.

4. Application of QD-MOF composites for photocatalysis

As a new type of composite photocatalyst, QD-MOF possesses high light stability, strong light adsorption capacity and fast photogenerated charge separation rate, which make these composites become an ideal photocatalyst. In this section, the applications of QD-MOF composites for photocatalysis are introduced, involving both energy production and environment remediation. And the detail applications of these composites are listed in Table 1. Additionally, the photocatalytic mechanisms are also described in detail.

4.1 Energy production

4.1.1 Hydrogen production by water splitting

With the rapid development of industry, all over the world is confronting with the problems of environmental pollution and energy exhaustion [141, 142]. In consideration of the cleanliness, hydrogen is considered a laudable new energy since the only product is water. One kind of efficient method for hydrogen production is

photocatalysis water splitting that has been studied for several decades since Fujishima and Honda firstly carried out the photocatalysis water splitting experiments in 1972 [143]. The composites of QDs integrating with MOFs exhibit remarkable capacity for photocatalysis water splitting. However, due to the high overpotential in hydrogen production, additional co-catalysts are often needed to decrease the overpotential and to help achieve hydrogen evolution [144, 145]. The overall process of water splitting includes two half-reactions, oxygen evolution and hydrogen evolution. The hydrogen evolution was more common than oxygen evolution. He and co-workers [109] synthesized CdS/MIL-101 by the method of “ship-in-a-bottle” and the noble metal Pt was loaded on the surface of CdS as co-catalyst by photodeposition. Due to the excellent visible light response of CdS and the remarkable stability of MIL-101 as well as the synergistic effect between CdS and MIL-101, the synthesized type-II heterojunction photocatalyst showed high photocatalytic activity. The energy band alignment of the heterojunction is shown as Fig. 6a. The maximum hydrogen evolution rate of CdS/MIL-101 under visible-light in lactic acid aqueous was detected as about $150 \mu\text{mol}\cdot\text{h}^{-1}$, higher than pure CdS. Under the same conditions, the photocatalytic activity of CdS/MOF-5 was investigated. However, this composite was not so effective due to the instability of MOF-5 in air, water and thermal treatment. Saha et al. [146] also embedded uncapped CdS QDs in ZAVCl-MOF and used Pt as a co-catalyst to solve the sluggish reaction kinetic of the obtained photocatalyst. Moreover, ethanol was used as a sacrificial reagent to expend photoinduced holes, protecting the photocatalyst from photo-corrosion. The hydrogen

production efficiency of CdS@ZAVCl-MOF reached to 398~418 $\mu\text{mol}\cdot\text{h}^{-1}\text{g}^{-1}$ under visible light and 500~510 $\mu\text{mol}\cdot\text{h}^{-1}\text{g}^{-1}$ with the presence of UV light.

In addition to the binary photocatalyst system, the ternary photocatalyst system also attracted the attention of researchers. Due to a low Fermi level, carbon based materials were ideal materials acted as electron library to combine with QDs and MOFs to form ternary composite. For instance, Meng and co-workers [119] co-encapsulated CDs and CdS QDs in the matrix of MIL-101. The obtained CD/CdS@MIL-101 material showed stronger light capture ability than single component CdS and binary CdS@MIL-101. The photocatalytic activity for hydrogen evolution of obtained CD/CdS@MIL-101 material was 14.66 $\mu\text{mol}\cdot\text{h}^{-1}$, which was 18.6 and 8.5 times of that of single component CdS and binary CdS@MIL-101, respectively. Lin et al. [129] synthesized a ternary composite material UiO-66/CdS/RGO (RGO represented reduced graphene oxide) by “photodeposited method” and the photocatalytic hydrogen evolution capacity of the composite was compared with binary UiO-66/CdS and ternary P25/CdS/RGO (P25 was commercial TiO₂ photocatalyst) composites. The results showed that the hydrogen production rate of UiO-66/CdS/RGO reached to 13.8 $\mu\text{mol}\cdot\text{h}^{-1}$, which was 13.8, 1.2 and 2 times of commercial CdS, UiO-66/CdS and P25/CdS/RGO respectively. In the same way, CdS@NU-1000/RGO was prepared and the hydrogen production efficiency was 2.42 $\text{mmol}\cdot\text{g}^{-1}\text{h}^{-1}$, higher than CdS and CdS@NU-1000 that were 0.2 $\text{mmol}\cdot\text{g}^{-1}\text{h}^{-1}$ and 1.87 $\text{mmol}\cdot\text{g}^{-1}\text{h}^{-1}$, severally [147]. In the CD/CdS@MIL-101, UiO-66/CdS/RGO, and CdS@NU-1000/RGO ternary composite systems, CdS QDs acted as light trapping

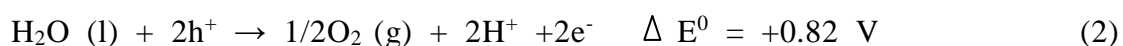
agent to absorb visible light and were excited to produce photoinduced electrons. After that, the electrons were transferred to the MOFs and then get to the CDs or RGO sheet for hydrogen evolution. The probable reason for the enhanced photocatalytic ability was that the large specific surface area of MOF provided more catalytic sites for CdS QDs that can effectively absorb light radiation, and the introduction of CDs or RGO accelerated the electron transmission and inhibited the photogenerated charge recombination, leading to the improvement of photocatalysis performance. Slightly differently, Jin and co-workers [141] designed MoS₂ QDs/UiO-66-NH₂/G composite by the method of “bottle-around-the-ship”. And the Eosin Y (EY) was used as sensitizer in the catalytic process. The photocatalytic hydrogen generation ability of EY-sensitized MoS₂ QDs/UiO-66-NH₂/G was tested under visible light irradiation with triethanolamine (TEOA) as sacrificial reagent. The result showed that hydrogen production activity was increased due to the synergetic effect of MoS₂ QDs and graphene together with UiO-66-NH₂. In this work, MoS₂ QDs acted as both catalyst and co-catalyst for the photocatalysis, and the graphene acted as a co-catalyst to provide a high specific surface area to induce fleetly electron migration, which achieved effective electron separation. And the quantum confinement of MoS₂ QDs supplied dangling bonds on surface and edges, which could aggregate photoinduced electrons leading a higher activity for hydrogen evolution. Compared with the UiO-66/CdS/RGO and CdS@NU-1000/RGO composites (Fig. 6b), the photocatalytic mechanism of hydrogen evolution by EY-sensitized MoS₂ QDs/UiO-66-NH₂/G showed some differences, which was

mainly reflected in the electron transport path (Fig. 6c). Under the irradiation of visible light, the EY absorbed light photons to generate singlet excited state EY^{1*} and further turned into lowest-lying triplet excited state EY^{3*} through a wonderful intersystem crossing. Then the EY^{3*} was quenched by TEOA and induced the production of reductive $EY^{\cdot-}$ and oxidative donor ($TEOA^+$). The $EY^{\cdot-}$ species firstly reached to the surface of UiO-66-NH₂ and followed reached to graphene, finally arrived at MoS₂ QDs, where the protons were reduced to produce hydrogen molecules. Meanwhile, the $EY^{\cdot-}$ species converted back to EY and the water reduction reaction was accomplished. Moreover, EY-sensitized MoS₂ QDs could also reduce H⁺ ions to produce hydrogen molecules. In this composite, the benzene rings of the EY and UiO-66-NH₂ constituted a strong π - π stacking and van der Waals force, facilitating the efficient transport of photogenerated electrons. Additionally, the effect of pH on water splitting was investigated and the results showed that the acidic and strongly basic conditions were unbeneficial for hydrogen evolution. The possible reason was that more H⁺ toward lead to a protonation of sacrificial agents triethanolamine (TEOA), resulting in an ineffective electron donor in acidic condition, thus to decrease the hydrogen production. In a strong basic condition, lower concentration of H⁺ caused a low thermodynamic driving force for photocatalysis. Therefore the optimum condition for hydrogen evolution was under neutral condition.

In addition to photocatalysis, the composites of QD-MOF also have been used in the field of photoelectrocatalytic water splitting [148]. Vaddipalli and co-workers [149] studied the preparation of Au NPs/CdSe/LaBTC composite photoanode and

further turned it into Au NPs/CdS/LaBTC MOF via exchanging selenium ions of CdSe with sulfide ions in the Na₂S solution during the photochemical oxidation process (Fig.7a). The color of photoanode changed from dark red to dark brown after the change of Au NPs/CdS/LaBTC to Au NPs/CdSe/LaBTC. The transformation of CdSe QDs to CdS nanosheet promoted the photoelectrochemical activity of water splitting due to an efficient generation of photoinduced electron-hole pairs and faster transfer of interface electrons. Besides, Au nanoparticles played a crucial part in photoelectrocatalytic hydrogen production due to the localized surface plasmon resonance, which led to effective photons absorption and electrons separation (Fig.7b). Therefore, the photocurrent intensity was increased to promote the reduction of H⁺ to H₂ on the counter electrode. The hydrogen production capacity of Au NPs/CdSe/LaBTC electrode was 3.2 mmol·(cm²)⁻¹, and the photoelectrode of Au NPs/CdSe/LaBTC was 2.6 times of CdSe/LaBTC electrode.

Water splitting is an uphill reaction that need to input energy to launch the reaction (eqn (1)). Therefore, the photons with energy greater than or equal to the photocatalyst band gap is the key to stimulate the photocatalytic reaction. The water splitting involves two equations (eqn (2) and eqn (3)) [150, 151].



Therefore, an effective photoelectron generation is required for photocatalytic hydrogen production. In the literatures of QD-MOF composites for photocatalysis

water splitting, QDs effectively capture photons in the visible region, and MOFs accelerate electrons separation and transport. Then, the co-catalysts, such as Pt, CDs, RGO and graphene were used to promote photogenerated charges separation and provide the reaction sites as well as decrease the activation energy for hydrogen production, thus to promote hydrogen production efficiency. Remarkably, a ternary system increases the decay path of excited state electrons and accelerates the rate of electron separation and hydrogen generation rate. The general mechanism of hydrogen production is shown in Fig. 8. Under the light radiation, photoinduced electrons generated from the CB of the QD-MOF composites are transferred to the co-catalyst surface to reduce hydrogen ions to produce hydrogen. At the same time, the remaining holes oxidize water molecules to produce oxygen or are consumed by hole scavengers.

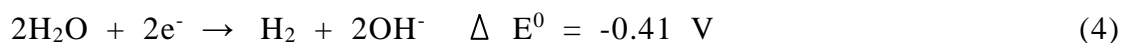
4.1.2 CO₂ reduction to produce CH₄ and/or CO

Combustion of large quantities of fossil fuels results in too much CO₂ emission, which is the main reason of Greenhouse Effect [152]. Converting CO₂ into chemical fuels (e.g. CO and CH₄, etc) by photocatalysis is considered an effective approach to decrease the amount of CO₂ [153, 154]. In the photocatalytic gas reaction, in addition to the high quantum efficiency, effective gas molecule capturing and activation on catalytic sites are also the main limiting factors [155]. The large surface area and adjustable pore structure of MOFs provide favorable conditions for gas adsorption [156]. Therefore, MOFs can be an ideal material for CO₂ reduction [157]. In the last

few decades, MOF-based photocatalysts have been used for CO₂ reduction. Recently, several researchers have studied the transformation of CO₂ into CH₄ and/or CO by using QD-MOF composites. For example, Li et al. [111] deposited TiO₂ nanoparticles on the surface of HKUST-1 to prepared core-shell HKUST-1@TiO₂. The synthesized composite showed selectivity for the reduction of CO₂ to CH₄. This selectivity was derived from the activation sites of the reduction reaction and the electron separation rate. HKUST-1 formed an activated catalyst after receiving the electrons of TiO₂. Subsequently, CO₂ molecules adsorbed at the Cu site was activated by the charged HKUST-1, which was a key step of CO₂ reduction. The evolution efficiency of CH₄ was 2.64 μmol·g⁻¹ h⁻¹ by using HKUST-1@TiO₂, more than 5 times that of pure TiO₂ (Fig. 9a). Kong et al. [158] grew ZIF-8 and ZIF-67 on the surface of CsPbBr₃ QDs to obtained the CsPbBr₃@ZIF composite with water stability and fast photoinduced electrons transmission as well as favourable CO₂ capture ability. Compared with ZIF-8, the combination of CsPbBr₃ with ZIF-67 showed better CO₂ reduction capacity. The reason was ascribed that ZIF-67 could respond to light radiation and more photoinduced electron-hole pairs was generated. Moreover, the Co center in ZIF-67 acted as an electron library to accelerate the separation of photoinduced carriers. After accepting the electrons from CsPbBr₃ and organic linkers, the Co(II) was activated. Subsequently, CO₂ was activated and reduced at the activated active site. Although no light capture capability has been exhibited, ZIF-8 can be a good electron acceptor or CO₂ capture agent. Therefore, the CsPbBr₃@ZIF-8 exhibited higher photocatalytic activity than pure CsPbBr₃. In the whole reaction process, only CO and CH₄ were

detected, and the yield of CH₄ was much higher than that of CO, indicating the reduction selectivity of CO₂ to CH₄ (Fig. 9b). The selectivity was realized by gas-catalyzed condition in which water vapor produced enough protons to provide adequate help to conquer dynamic barriers for CH₄ formation. Additionally, Wan et al. [137] also synthesized CsPbBr₃ QDs UiO-66(NH₂) nanojunction for CO₂ reduction. However, different from the HKUST-1@TiO₂ and CsPbBr₃@ZIF, this composite showed the selectivity of CO instead of CH₄. The reason was explained as that CO₂ converse to CO was a 2-electron process, whereas it was an 8-electron process for CH₄. Thus it was easier to produce CO than to produce CH₄. The yields of CH₄ and CO were continue to rise and the total output reached to 3.08 and 98.57 μmol·g⁻¹ (Fig. 9c). The corresponding production rate were 0.26 μmol·g⁻¹ h⁻¹ and 8.21 μmol·g⁻¹ h⁻¹ respectively.

The probable mechanism of photocatalytic reduction of CO₂ is demonstrated as Fig. 9d. Under the light radiation, QDs are photoexcited to generate charge carriers and the photoinduced electrons are transferred to MOFs due to the matched band potentials and excellent interfacial contact. The reduction process of CO₂ refers to followed equations:



In addition, the active holes in VB oxidize H₂O to produce O₂ and H⁺ by the followed oxidation reaction:



This oxidation process consumes the photoproduction holes, restraining the charges recombination, thus to maintain the efficient operation of photocatalytic reaction.

4.2 Environmental remediation

4.2.1 Organic dye degradation

Industrial wastewater contains quantities of organic pollutants, and dye is one of the main organic pollutants, which have adverse effects on the ecological environment [159-161]. Photocatalysis as an efficient method has been widely used in industrial wastewater treatment [162]. The QD-MOF materials with strong light capturing ability and fast electron separation rate are ideal photocatalysis for wastewater treatment, and most of the research focuses on dye degradation. So far, it mainly involves the degradation of rhodamine 6G (Rh 6G), rhodamine B (RhB) and MB and so on. Kaur and peers [163, 164] encapsulated the prepared CdTe QDs into the matrix of Eu-MOF and NTU-9 by the method of bottle around the ship. The CdTe QDs/NTU-9 showed faster degradation rate than CdTe QDs/Eu-MOF due to the improvement of photodegradation kinetics. NTU-9 had a higher specific surface area and larger pore volume than Eu-MOF, which provided more adsorption sites for dye molecules and thus exhibited higher degradation ability. The effect of pH on degradation efficiency of Rh 6G also studied and the result showed that, lower pH conditions were favorable to improve the photocatalysis activity of dye degradation. The reason was explained as that, under acidic conditions, hydrogen peroxide

promoted the production of hydroxyl radicals, thus accelerating the degradation of dyes. Huang et al. [132] also investigated the effect of pH on MB and RhB degradation by using N-doped TiO₂/MIL-100(Fe). Differently, the result showed that, in acidic or alkaline condition, the catalysis efficiency was damaged due to dye desorption and catalyst active site corrosion. Gan et al. [110] incorporated CdSe QDs with UiO-66 and the degradation rate of RhB reached to 100% within 50 minutes under acidic conditions. Huang et al. [135] also prepared CdSe QDs sensitized MIL-125(Ti)/TiO₂@SiO₂ two-level type-II heterostructure and the composite showed strong degradation ability of RhB. Regrettably, due to the low oxidation capacity, RhB could not be completely oxidized into CO₂ and H₂O but produced tartaric acid and 2-Hydroxyhexanedial. The energy band position and photocatalytic mechanism of this two-level type-II heterostructure is shown as Fig 10a. In order to increase the light capture ability and stability of MIL-125(Ti), Wang et al. [120] modified MIL-125(Ti) with the amino groups to obtain NH₂-MIL-125(Ti). Then the CQDs with size of 2 nm were deposited on the surface of NH₂-MIL-125(Ti). The prepared CQDs/NH₂-MIL-125(Ti) composite exhibited a better respond in visible region compared to pure NH₂-MIL-125(Ti) and even respond to near-infrared light area due to narrowing of the band gap of NH₂-MIL-125(Ti) after introducing CQDs. After receiving photon radiation, the CQDs converted near-infrared light to visible-light by upconversion and to activate NH₂-MIL-125(Ti) (Fig. 10b). Therefore, the effective absorption of light energy leaded to produce more photogenerated charges to promote the photodegradation capacity for RhB.

In the process of photocatalytic dye degradation, the adsorption of dye molecules and the activity of photocatalyst are the main factors determining the degradation rate of dyes [165, 166]. The large specific surface area of MOFs provide conditions for dye adsorption, and QDs enhance light trapping ability and reduce the recombination rate of photogenerated charges, thus achieves effective dye degradation. In addition, pH also is one of the factors that cannot be ignored in dye degradation. Different pH will affect the structure of the dyes, the electrostatic interaction between dye molecules, the performance of the catalysts and the type of reactive radicals, thereby affecting the photocatalytic activity. The basic mechanism of photocatalytic dye degradation is shown as Fig. 10c, the h^+ (hole) and $\cdot O_2^-$ (superoxide radical) are the main potential substances, and the photocatalytic mechanism involves the following equations:



4.2.2 Cr(VI) reduction

As one of the main environmental pollutants, Cr(VI) reduction have been a research hotspot in environmental remediation [167]. Accumulation of Cr (VI) in soil and living organisms has adverse effects on ecosystem and poses a threat to human health [168]. Photogenerated electrons with strong reducibility can effectively reduce

Cr(VI) to Cr(III). Therefore numerous photocatalysts have been used to repair wastewater of Cr(VI) pollution [169]. QD-MOF materials with superior photocatalytic capacity have also been used for Cr(VI) removal [170, 171]. Due to the remarkable photoresponsiveness of metal sulfide nanoparticles, Yuan et al. [130] deposited metallic sulfide QDs (Ag_2S , CdS and CuS QDs) on the surface of MIL-125 (Ti) via in situ “photodeposition” method under ultraviolet light condition. These synthesized composites have visible light responsiveness and show excellent photocatalytic ability for Cr(VI) reduction under acidic conditions. The UV-vis spectrum indicated that MIL-125(Ti) achieved a wider spectral absorption range after the introduction of QDs. The promoting of photocatalytic activity was resulted from the introduction of a narrow band gap semiconductor, which enhanced the photosensitive ability and light trapping ability. The heterojunction between QDs and MIL-125 (Ti) improved the efficiency of charges separation, inhibiting the recombination of photogenic electron pairs. Therefore, the photocatalytic reduction ability of Cr(VI) was improved. Recently, low toxicity CQDs were also encapsulated in the cavities of MIL-53 (Fe) by “ship-in-the-bottle” method [140]. The photocatalysis activity of the prepared composite for Cr(VI) reduction was investigated under pH range from 3 to 7. The results showed that photocatalytic activity was better when the pH values were 3~4 and the optimal pH value was 4. The reason was that under acidic condition, Cr(VI) existed in the form of $\text{Cr}_2\text{O}_7^{2-}$, which was conducive to reduce to Cr^{3+} . Under alkaline condition, Cr(VI) ions existed in the form of $\text{Cr}(\text{OH})_3$ colloid, which may cover the surface of the photocatalyst, resulting

in the light absorption capacity of photocatalyst and the opportunities of Cr(VI) ions contact with photocatalyst were reduced, thus leading to a decrease in catalytic activity. The introduction of CQDs improved the photocatalytic ability of MIL-53 (Fe) significantly, and the photocatalytic ability of the composite can be adjusted by controlling the content of CQDs. The overloading of CQDs shield the incident light, resulting in the decrease of photocatalytic activity. The main reason for the enhanced photocatalytic activity of the composite was that CQDs can be used as electron acceptor to promote the separation of photogenic carriers. In addition, CQDs played a role of photosensitizer, that absorbed long-wavelength visible light (>570 nm) and transmitted energy to MIL-53 (Fe), enhancing the light absorption in long-wavelength visible light regions and resulting in a promotion of photocatalytic performance.

In the two examples above, photocatalytic mechanisms showed slight differences. In the first literature, as the main light-responsive material, metallic sulfide QDs generated photogenerated electrons, and MIL-125 (Ti) accelerated electron separation (Fig. 11a). In the second literature, CQDs were not the desired photocatalyst. Instead, MIL-53 (Fe) showed higher Cr(VI) photoreduction activity. CQDs acted as electron acceptors to accept photogenerated electrons from MIL-53 (Fe) and inhibited photogenerated charges recombination (Fig. 11b).

4.2.3 Nitric oxide oxidation

Air pollution has aroused world great concern. Nitric oxide (NO) as one of the major air pollutants, mainly derives from vehicle emissions and fossil fuel combustion

[172]. NO reacts with O₂ to form toxic NO₂ and N₂O₄, causing secondary pollution [173]. In addition, NO is the main source of acid rain and photochemical smog, which seriously impacts the ecological environment [174]. Recently, MOF-based photocatalysis coupled with QDs has been used for NO removal. Gao et al.[175] suggested a facile one-step strategy for gap modification of NH₂-MIL-125 by coating a thin layer of TiO₂ nanoparticles, promoting visible light absorption. Further coupled with co-catalyst CdS QDs to synthesize CdS QDs/NH₂-MIL-125@TiO₂ ternary composite. Due to the production of more radicals, the as-synthesized composite showed higher photocatalytic activity for NO oxidation compared to pure NH₂-MIL-125. According to the HOMO/LUMO energy of NH₂-MIL-125 and VB/CB of pure TiO₂ and CdS QD, the mechanism of photocatalytic NO oxidation is demonstrated in Fig. 12. Under the visible light, both NH₂-MIL-125 and CdS QDs generated photogenerated electrons, which were rapidly transferred to TiO₂ and reacted with O₂ to generate ·O₂⁻, further generating ·OH. Meanwhile, h⁺ also promoted the generation of ·OH. Subsequently, both ·OH and ·O₂⁻ oxidized NO to NO₃⁻. The oxidation process referred to the following equations:





In this oxidation process, $\cdot\text{OH}$ (hydroxyl radical) and $\cdot\text{O}_2^-$ were the main active groups for NO oxidation. Distinctly, the oxidation of NO involved the production of nitrates and nitrites, which would damage the structure of NH₂-MIL-125. Hence the TiO₂ nanoparticles on NH₂-MIL-125 surface played a shield role to prevent MOFs from corrosion and poisoning. Moreover, hydrophilicity and porosity promoted the diffusion and penetration of Cd²⁺ and S²⁻ into the micropores of TiO₂. Sequentially, CdS QDs were immobilized on the surface of TiO₂ and the intimate interface between them led to a rapid electron separation, which ensured the remarkable photocatalysis performance for CdS QDs@NH₂-MIL-125. The photocatalytic efficiency of the composite material to NO reached 48.5%, higher than that of single NH₂-MIL-125 (30.9%) and NH₂-MIL-125@TiO₂ (32.8%).

5. Summary and perspective

MOFs have been used as admirable photocatalyst due to their unique structure and properties such as porosity, large internal surface area and abundant active sites. Combined with other materials, the photocatalytic ability of MOFs can be enhanced. Attributing to the quantum confinement effects, QDs possess excellent photocatalytic performance, including high quantum yield, low photobleaching, and wide absorption spectra and so on. The combination of QDs with MOFs exhibits an excellent photocatalytic capacity and physicochemical stability. In this review, we introduced

the structures, properties, synthesis methods of QD-MOF composites and summarized their applications in photocatalysis in recent few years, mainly involved the fields of energy production and environmental remediation, including water splitting for hydrogen production, CO₂ reduced to generate CH₄ and/or CO, organic dye degradation, Cr(VI) reduction and NO oxidation. Although the related researches of QD-MOF composites are still in the initial stage, the existing studies have indicated that this composite will have a bright future in photocatalysis field. In this composite system, MOFs and QDs play different roles respectively. The MOFs stabilize and disperse QDs, preventing QDs from aggregation, increasing the number of active sites and reducing the recombination rate of photogenic electron-hole pairs. QDs with narrow band gap expand the response range of the solar spectrum and increase the visible light capture capability of MOFs, and sometimes transmit light energy to the MOFs. Accordingly, QDs mainly play a role as photosensitizer to make MOFs more efficient use of visible light. The excellent properties of QDs and MOFs and the synergistic effect between them are the reasons for the enhanced photocatalytic ability. Although great progress has been made in the field of the QD-MOF-based photocatalysis, the application of such catalysts is still limited. In order to realize the application of these composites in practical production widely, a lot of efforts are needed.

(1) Extend the application of QD-MOF composites. In the field of organic pollution degradation, apart from organic dye, QD-MOF composites can also be applied to the removal of other organic pollutants, such as pesticides and antibiotics

that exist in large quantities in the environment. Besides, the application of QD-MOF composites in heavy metal removal is extremely rare. Cr(VI) is the only heavy metal ion is studied by using this composites. Therefore, expanding the application scope of QD-MOF composites is needed.

(2) Control the growth of QDs precisely and construct the form of MOFs. In the current methods of synthesizing QD-MOF composites, the growth sites of QDs are random, such as "ship-in-the-bottle" method, the shape, size and growing spots of QDs are difficult to control. Although the size of QDs can be regulated by adjusting the ratio of precursors, reaction time and temperature, it is not a simple process but complex and contingent. Through continuous trial and improve experimental conditions, it may be possible to achieve control of QDs morphology. As for controlling the growth site of QDs on MOFs, it can be considered to adjust the position of functional groups on the organic linkers of MOFs and modify QDs surface with specific ligand. Then, precise growth of the QDs may be achieved by the interaction force between the functional groups. In addition, in the "bottle-around-the-ship" method, the structures of MOFs are affected because of the distribution of QDs, that make it is difficult to ensure the conformal shape of MOFs. Therefore, optimizing existing synthesis methods or developing new synthesis methods is one of the next research points.

(3) Study environmental tolerance of QD-MOF composites. Research on the adaptability of QD-MOF composites to the environment is a prerequisite for the shift from laboratory research to practical application. The catalytic activity of the

photocatalyst is not only affected by its own properties, but also affected by the application environment. Such as temperature, pH, contaminant and so on. Although there is no relevant research at present, it can be envisaged that whether the QD-MOF materials could be encapsulated or coated to enhance their resistance so as to maintain their tolerance to environment. Further researches can be explored along these lines.

(4) Environmental risk assessment and recovery of QD-MOF composites. The components of some MOFs and QDs contain heavy metal element, which may result in secondary pollution during application. This is one of the main reasons limited their application in environmental remediation. Therefore, it is necessary to develop new types of MOFs and QDs with low toxicity and low environmental hazard. At present, carbon-based QDs (e.g., CQDs, GQDs, etc.) are ideal photocatalytic materials due to non-toxic properties. In addition, the researches on the recovery and degradation of MOFs and QDs should also attract the attention of follow-up studies. In general, QD-MOF composites, as a type of emerging photocatalyst, has strong photocatalytic properties. Although these composites still have many challenges in practical applications, their excellent photocatalytic properties make it a promising prospect.

(5) Further explore the photogenerated electron transmission path. In the composite photocatalysts containing co-catalysts, the transport path of photogenerated electrons is closely related to the energy band position and contact mode of each component. When the components are in intimate contact and the band gap is matched, there may be multiple photogenerated electron transport paths [176]. The most common pathway is that the photogenerated electrons are transferred from the

component that with most negative CB edge to other components with more positive CB edges step by step and finally reach the co-catalyst. Besides, there is also a path that when the photogenerated electrons are transferred step by step, some photoelectrons can be directly transferred to the co-catalyst [177-179]. Despite many studies have shown that multipath electron transport exists in multiple photocatalyst, the researches on whether there is competitive photogenerated electron absorption between co-catalysts and QDs in the QD-MOF composites loaded with co-catalysts are still lacked. Therefore, a further research is urgently needed.

(6) Further determining the characteristics of photocatalytic redox reaction of each component in the composites. Whether the photocatalytic redox reaction can be carried out is not only related to the position of the energy band but also related to the reaction kinetics [180]. When the CB/VB position of the component in the composite material is higher/lower than the required reduction/oxidation potential, then this component cannot undergo reduction/oxidation reaction. In addition, due to the difference in energy band between the each components of the composite, the photogenerated electrons and holes will be migrated. Besides, a small part of the holes/electrons that are not migrated will be recombined at a nanosecond speed. Thus the amount of untransferred electrons/holes remaining on each component is very small, so that the reduction/oxidation reaction may not be driven. Therefore, generally speaking, the probability of occurring oxidation and reduction reactions of each component of the composite materials simultaneously is very small. Although, most studies show that the oxidation reactions and reduction reactions will take place on

the rich-hole component and rich-electron component respectively [180, 181], further studies are needed to determine whether each component in the composite can be active for oxidation and reduction reactions simultaneously.

Acknowledgements

The study was financially supported by the Program for Changjiang Scholars and Innovative Research Team in University (IRT-13R17), the National Natural Science Foundation of China (51679085, 51378192, 51039001, 51378190, 51521006, 51508177), the Fundamental Research Funds for the Central Universities of China (No.531107050930), China Postdoctoral Science Foundation Funded Project (2018M642977), the Funds of Hunan Science and Technology Innovation Project (No. 2018RS3115).

References

- [1] K. Nakata, A. Fujishima, J. Photochem. Photobiol. C-Photochem. Rev., 13 (2012) 169-189.
- [2] B.B. Shao, Z.F. Liu, H. Zhong, G.M. Zeng, G.S. Liu, M.D. Yu, Y. Liu, X. Yang, Z.G. Li, Z.D. Fang, J.T. Zhang, C.H. Zhao, Microbiol. Res., 200 (2017) 33-44.
- [3] Y. Liu, M. Cheng, Z. Liu, G. Zeng, H. Zhong, M. Chen, C. Zhou, W. Xiong, B. Shao, B. Song, Chemosphere, 236 (2019) 124387.
- [4] S. Garcia-Segura, E. Brillas, J. Photochem. Photobiol. C-Photochem. Rev., 31 (2017) 1-35.
- [5] Y. Pi, X. Li, Q. Xia, J. Wu, Y. Li, J. Xiao, Z. Li, Chem. Eng. J., 337 (2018) 351-371.
- [6] Z.Y. Lin, L.H. Li, L.L. Yu, W.J. Li, G.W. Yang, PCCP, 19 (2017) 8356-8362.
- [7] Z. Liu, B. Shao, G. Zeng, M. Chen, Z. Li, Y. Liu, Y. Jiang, H. Zhong, Y. Liu, M. Yan, Chemosphere, 210 (2018) 922-930.
- [8] L. Wang, J. Zhao, H. Liu, J. Huang, J. Taiwan Inst. Chem. Eng., 93 (2018) 590-602.
- [9] S.L. Lee, C.-J. Chang, Polymers, 11 (2019).
- [10] Z.-J. Shi, M.-G. Ma, J.-F. Zhu, Catalysts, 9 (2019).
- [11] Q. Liang, X. Liu, G. Zeng, Z. Liu, L. Tang, B. Shao, Z. Zeng, W. Zhang, Y. Liu, M. Cheng, W. Tang, S. Gong, Chem. Eng. J., 372 (2019) 429-451.
- [12] M. Yu, Z. Liu, G. Zeng, H. Zhong, Y. Liu, Y. Jiang, M. Li, X. He, Y. He, Carbohydr. Res., 407 (2015) 63-72.
- [13] B. Bajorowicz, M.P. Kobylanski, A. Golabiewska, J. Nadolna, A. Zaleska-Medynska, A. Malankowska,

- Adv. Colloid Interface Sci., 256 (2018) 352-372.
- [14] L. Shen, R. Liang, L. Wu, Chin. J. Catal., 36 (2015) 2071-2088.
- [15] Y. Liu, Z. Liu, D. Huang, M. Cheng, G. Zeng, C. Lai, C. Zhang, C. Zhou, W. Wang, D. Jiang, H. Wang, B. Shao, Coord. Chem. Rev., 388 (2019) 63-78.
- [16] B. Shao, Z. Liu, G. Zeng, Z. Wu, Y. Liu, M. Cheng, M. Chen, Y. Liu, W. Zhang, H. Feng, ACS Sustainable Chem. Eng., 6 (2018) 16424-16436.
- [17] B. Shao, X. Liu, Z. Liu, G. Zeng, W. Zhang, Q. Liang, Y. Liu, Q. He, X. Yuan, D. Wang, S. Luo, S. Gong, Chem. Eng. J., 374 (2019) 479-493.
- [18] M.R. Gholipour, D. Cao-Thang, F. Beland, D. Trong-On, Nanoscale, 7 (2015) 8187-8208.
- [19] B. Shao, X. Liu, Z. Liu, G. Zeng, Q. Liang, C. Liang, Y. Cheng, W. Zhang, Y. Liu, S. Gong, Chem. Eng. J., 368 (2019) 730-745.
- [20] T. Uekert, M.F. Kuehnel, D.W. Wakerley, E. Reisner, Energy Environ. Sci., 11 (2018) 2853-2857.
- [21] Y.-S. Fu, J. Li, J. Li, Nanomaterials, 9 (2019).
- [22] N. Zhang, S. Liu, Y.-J. Xu, Nanoscale, 4 (2012) 2227-2238.
- [23] Y.-W. Su, W.-H. Lin, Y.-J. Hsu, K.-H. Wei, Small, 10 (2014) 4427-4442.
- [24] G. Huang, Y. Chen, H. Jiang, Acta Chim. Sinica, 74 (2016) 113-129.
- [25] Q. Pang, B. Tu, Q. Li, Coord. Chem. Rev., 388 (2019) 107-125.
- [26] X. Liu, B. Tang, J. Long, W. Zhang, X. Liu, Z. Mirza, Sci. Bull., 63 (2018) 502-524.
- [27] Y. Xu, Q. Li, H. Xue, H. Pang, Coord. Chem. Rev., 376 (2018) 292-318.
- [28] A. Dhakshinamoorthy, A.M. Asiri, H. Garcia, Angew. Chem. Int. Ed. Engl., 55 (2016) 5414-5445.
- [29] K.V. Vokhmintcev, P.S. Samokhvalov, I. Nabiev, Nano Today, 11 (2016) 189-211.
- [30] L. Cui, C.-c. Li, B. Tang, C.-y. Zhang, Analyst, 143 (2018) 2469-2478.
- [31] M. Geszke-Moritz, M. Moritz, Mater. Sci. Eng., C, 33 (2013) 1008-1021.
- [32] Q.L. Zhu, Q. Xu, Chem. Soc. Rev., 43 (2014) 5468-5512.
- [33] S. Rajaambal, K. Sivaranjani, C.S. Gopinath, J. Chem. Sci., 127 (2015) 33-47.
- [34] C. Ma, M. Zhou, D. Wu, M. Feng, X. Liu, P. Huo, W. Shi, Z. Ma, Y. Yan, CrystEngComm, 17 (2015) 1701-1709.
- [35] M. Shamsipur, H.R. Rajabi, Spectrochim. Acta, Part A, 122 (2014) 260-267.
- [36] J. Aldana, Y.A. Wang, X. Peng, JACS, 123 (2001) 8844-8850.
- [37] Y. Liu, Z. Liu, G. Zeng, M. Chen, Y. Jiang, B. Shao, Z. Li, Y. Liu, J. Hazard. Mater., 357 (2018) 10-18.
- [38] P.A. Gale, N. Busschaert, C.J. Haynes, L.E. Karagiannidis, I.L. Kirby, Chem. Soc. Rev., 43 (2014) 205-241.
- [39] L. Zhang, L. Yin, C. Wang, N. Lun, Y. Qi, ACS Appl. Mater. Interfaces, 2 (2010) 1769-1773.
- [40] A.A.P. Mansur, H.S. Mansur, F.P. Ramanery, L.C. Oliveira, P.P. Souza, Appl. Catal. B-Environ., 158-159 (2014) 269-279.
- [41] H.R. Rajabi, O. Khani, M. Shamsipur, V. Vatanpour, J. Hazard. Mater., 250-251 (2013) 370-378.
- [42] M. Shamsipur, H.R. Rajabi, Spectroc. Acta Pt. A-Molec. Biomolec., 122 (2014) 260-267.
- [43] H.R. Rajabi, M. Farsi, Mater. Sci. Semicond. Process., 31 (2015) 478-486.
- [44] A. Samadi-Maybodi, M.-R. Sadeghi-Maleki, Spectroc. Acta Pt. A-Molec. Biomolec., 152 (2016) 156-164.
- [45] J.-J. Shi, S. Wang, T.-T. He, E.S. Abdel-Halim, J.-J. Zhu, Ultrason. Sonochem., 21 (2014) 493-498.
- [46] S.Y. Choi, J.P. Shim, D.S. Kim, T. Kim, K.S. Suh, J. Nanomater., (2012).
- [47] A.R. Kortan, R. Hull, R.L. Opila, M.G. Bawendi, M.L. Steigerwald, P.J. Carroll, L.E. Brus, JACS, 112 (1990) 1327-1332.

- [48] K.-G. Ma, J.-Y. Bai, T. Fang, H.-Q. Guo, *J. Nanosci. Nanotechnol.*, **14** (2014) 4940-4948.
- [49] A.A.P. Mansur, H.S. Mansur, F.P. Ramanery, L.C. Oliveira, P.P. Souza, *Appl. Catal. B-Environ.*, **158** (2014) 269-279.
- [50] H. Moon, C. Lee, W. Lee, J. Kim, H. Chae, *Adv. Mater.*, **31** (2019) e1804294.
- [51] Y. Fu, D. Kim, W. Jiang, W. Yin, T.K. Ahn, H. Chae, *RSC Adv.*, **7** (2017) 40866-40872.
- [52] F. Zhang, Z.-F. Shi, Z.-Z. Ma, Y. Li, S. Li, D. Wu, T.-T. Xu, X.-J. Li, C.-X. Shan, G.-T. Du, *Nanoscale*, **10** (2018) 20131-20139.
- [53] C. Zhou, H. Shen, Y. Guo, L. Xu, J. Niu, Z. Zhang, Z. Du, J. Chen, L.S. Li, *J. Colloid Interface Sci.*, **344** (2010) 279-285.
- [54] J.H. Kim, J. Park, N. Won, H. Chung, S. Kim, *J. Exp. Nanosci.*, **4** (2009) 105-112.
- [55] L.D. Field, S.A. Walper, K. Susumu, G. Lasarte-Aragones, E. Oh, I.L. Medintz, J.B. Delehanty, *Bioconjugate Chem.*, **29** (2018) 2455-2467.
- [56] A. Sangtani, E. Petryayeva, M. Wu, K. Susumu, E. Oh, A.L. Huston, G. Lasarte-Aragones, I.L. Medintz, W.R. Algar, J.B. Delehanty, *Bioconjugate Chem.*, **29** (2018) 136-148.
- [57] A. Kumari, A. Sharma, U. Malairaman, R.R. Singh, *J. Lumin.*, **199** (2018) 174-182.
- [58] J. Yao, P. Li, L. Li, M. Yang, *Acta Biomater.*, **74** (2018) 36-55.
- [59] A. Nagy, K.B. Gemmill, J.B. Delehanty, I.L. Medintz, K.E. Sapsford, *IEEE J. Sel. Top. Quantum Electron.*, **20** (2014).
- [60] H. Zhou, J. Liu, S. Zhang, *Trac-Trends Anal. Chem.*, **67** (2015) 56-73.
- [61] K. Jung, J. Lee, Y.-M. Kim, Y.C. Park, M.-J. Lee, *Compos. Sci. Technol.*, **179** (2019) 79-87.
- [62] T.G. Kim, G.Y. Kwak, K. Do, K.J. Kim, *Nanotechnology*, **30** (2019).
- [63] L. Li, X. Hu, Y. Sun, X. Zhang, W. Jin, *Electrochem. Commun.*, **13** (2011) 1174-1177.
- [64] L. Tan, J. Ge, M. Jiao, G. Jie, S. Niu, *Talanta*, **183** (2018) 108-113.
- [65] K.-A. Tsai, Y.-J. Hsu, *Appl. Catal. B-Environ.*, **164** (2015) 271-278.
- [66] S. Sahai, A. Ikram, S. Rai, R. Shrivastav, S. Dass, V.R. Satsangi, *Renewable Sustainable Energy Rev.*, **68** (2017) 19-27.
- [67] S. Zhang, L. Wang, C. Liu, J. Luo, J. Crittenden, X. Liu, T. Cai, J. Yuan, Y. Pei, Y. Liu, *Water Res.*, **121** (2017) 11-19.
- [68] L. Jiao, Y. Wang, H.L. Jiang, Q. Xu, *Adv. Mater.*, **30** (2018).
- [69] R. Zhu, J. Ding, L. Jin, H. Pang, *Coord. Chem. Rev.*, **389** (2019) 119-140.
- [70] S. Wang, C.M. McGuirk, A. d'Aquino, J.A. Mason, C.A. Mirkin, *Adv. Mater.*, **30** (2018).
- [71] D. Bradshaw, A. Garai, J. Huo, *Chem. Soc. Rev.*, **41** (2012) 2344-2381.
- [72] S. Yuan, L. Feng, K. Wang, J. Pang, M. Bosch, C. Lollar, Y. Sun, J. Qin, X. Yang, P. Zhang, Q. Wang, L. Zou, Y. Zhang, L. Zhang, Y. Fang, J. Li, H.-C. Zhou, *Adv. Mater.*, **30** (2018).
- [73] Y. Li, Y. Xu, Y. Liu, H. Pang, *Small*, (2019) e1902463.
- [74] K.S. Park, Z. Ni, A.P. Cote, J.Y. Choi, R. Huang, F.J. Uribe-Romo, H.K. Chae, M. O'Keeffe, O.M. Yaghi, *Proc Natl Acad Sci U S A*, **103** (2006) 10186-10191.
- [75] B. Assfour, S. Leoni, G. Seifert, *J. Phys. Chem. C*, **114** (2010) 13381-13384.
- [76] J.H. Cavka, S. Jakobsen, U. Olsbye, N. Guillou, C. Lamberti, S. Bordiga, K.P. Lillerud, *J. Am. Chem. Soc.*, **130** (2008) 13850-13851.
- [77] R.J. Drout, L. Robison, O.K. Farha, *Coord. Chem. Rev.*, **381** (2019) 151-160.
- [78] A. Dhakshinamoorthy, A.M. Asiri, H. Garcia, *ACS Catal.*, **7** (2017) 2896-2919.
- [79] A. Malouche, C. Zlotea, P.A. Szilagy, *Chemphyschem*, **20** (2019) 1282-1295.
- [80] P. Ling, J. Lei, L. Zhang, H. Ju, *Anal. Chem.*, **87** (2015) 3957-3963.

- [81] B. Li, H.M. Wen, Y. Cui, W. Zhou, G. Qian, B. Chen, *Adv. Mater.*, 28 (2016) 8819-8860.
- [82] D. Li, S.-H. Yu, H.-L. Jiang, *Adv. Mater.*, 30 (2018).
- [83] P. Railey, Y. Song, T. Liu, Y. Li, *Mater. Res. Bull.*, 96 (2017) 385-394.
- [84] C.-X. Chen, Q.-F. Qiu, M. Pan, C.-C. Cao, N.-X. Zhu, H.-P. Wang, J.-J. Jiang, Z.-W. Wei, C.-Y. Su, *Chem. Commun.*, 54 (2018) 13666-13669.
- [85] S. Iram, M. Imran, F. Kanwal, S. Latif, Z. Iqbal, *Mater. Res. Express*, 6 (2019).
- [86] L. Li, Y. Liu, Y. Han, X. Qi, X. Li, H. Fan, L. Meng, *Mater. Lett.*, 236 (2019) 131-134.
- [87] X. Wei, Y. Li, H. Peng, D. Gao, Y. Ou, Y. Yang, J. Hu, Y. Zhang, P. Xiao, *Chem. Eng. J.*, 355 (2019) 336-340.
- [88] B. Zhu, D. Xia, R. Zou, *Coord. Chem. Rev.*, 376 (2018) 430-448.
- [89] S. Ishaq, R. Tamime, M.R. Bilad, A.L. Khan, *Sep. Purif. Technol.*, 210 (2019) 442-451.
- [90] L. Li, L. Guo, S. Pu, J. Wang, Q. Yang, Z. Zhang, Y. Yang, Q. Ren, S. Alnemrat, Z. Bao, *Chem. Eng. J.*, 358 (2019) 446-455.
- [91] A. Katoch, R. Bhardwaj, N. Goyal, S. Gautam, *Vacuum*, 158 (2018) 249-256.
- [92] A. Kirchon, L. Feng, H.F. Drake, E.A. Joseph, H.-C. Zhou, *Chem. Soc. Rev.*, 47 (2018) 8611-8638.
- [93] T. Simon-Yarza, A. Mielcarek, P. Couvreur, C. Serre, *Adv. Mater.*, 30 (2018).
- [94] K. Zhang, X. Meng, Y. Cao, Z. Yang, H. Dong, Y. Zhang, H. Lu, Z. Shi, X. Zhang, *Adv. Funct. Mater.*, 28 (2018).
- [95] X.-Y. Dong, J.-H. Wang, S.-S. Liu, Z. Han, Q.-J. Tang, F.-F. Li, S.-Q. Zang, *ACS Appl. Mater. Interfaces*, 10 (2018) 38209-38216.
- [96] J. Du, X. Sun, Y. He, Y. Yu, X. Zheng, L. Tian, Z. Liu, *Appl. Organomet. Chem.*, 32 (2018).
- [97] S. Wang, M. Wahiduzzaman, L. Davis, A. Tissot, W. Shepard, J. Marrot, C. Martineau-Corcus, D. Hamdane, G. Maurin, S. Devautour-Vinot, C. Serre, *Nat. Commun.*, 9 (2018).
- [98] S.N. Zhao, G. Wang, D. Poelman, P. Van Der Voort, *Molecules*, 23 (2018).
- [99] C. Wang, X. Liu, N.K. Demir, J.P. Chen, K. Li, *Chem. Soc. Rev.*, 45 (2016) 5107-5134.
- [100] A.B.P. Lever, *J. Chem. Educ.*, 51 (1974) 612-616.
- [101] S. Bauer, C. Serre, T. Devic, P. Horcajada, J. Marrot, G. Ferey, N. Stock, *Inorg. Chem.*, 47 (2008) 7568-7576.
- [102] T. Ahnfeldt, D. Gunzelmann, T. Loiseau, D. Hirsemann, J. Senker, G. Ferey, N. Stock, *Inorg. Chem.*, 48 (2009) 3057-3064.
- [103] S. Couck, J.F.M. Denayer, G.V. Baron, T. Remy, J. Gascon, F. Kapteijn, *JACS*, 131 (2009) 6326-+.
- [104] P. Serra-Crespo, E.V. Ramos-Fernandez, J. Gascon, F. Kapteijn, *Chem. Mater.*, 23 (2011) 2565-2572.
- [105] C.-C. Wang, X.-H. Yi, P. Wang, *Appl. Catal. B-Environ.*, 247 (2019) 24-48.
- [106] J. De Decker, K. Folens, J. De Clercq, M. Meledina, G. Van Tendeloo, G. Du Laing, P. Van Der Voort, *J. Hazard. Mater.*, 335 (2017) 1-9.
- [107] K. Wang, N. Li, J. Zhang, Z. Zhang, F. Dang, *Biosens. Bioelectron.*, 87 (2017) 339-344.
- [108] B.P. Biswal, D.B. Shinde, V.K. Pillai, R. Banerjee, *Nanoscale*, 5 (2013) 10556-10561.
- [109] J. He, Z. Yan, J. Wang, J. Xie, L. Jiang, Y. Shi, F. Yuan, F. Yu, Y. Sun, *Chem. Commun.*, 49 (2013) 6761-6763.
- [110] H. Gan, Z. Wang, H. Li, Y. Wang, L. Sun, Y. Li, *RSC Adv.*, 6 (2016) 5192-5197.
- [111] R. Li, J.H. Hu, M.S. Deng, H.L. Wang, X.J. Wang, Y.L. Hu, H.L. Jiang, J. Jiang, Q. Zhang, Y. Xie, Y.J. Xiong, *Adv. Mater.*, 26 (2014) 4783-+.
- [112] X.-Y. Xu, B. Yan, *J. Mater. Chem. A*, 5 (2017) 2215-2223.

- [113] J.-X. Wu, B. Yan, Dalton Trans., 46 (2017) 7098-7105.
- [114] D. Kandi, S. Martha, K.M. Parida, Int. J. Hydrogen Energy, 42 (2017) 9467-9481.
- [115] J.B. DeCoste, G.W. Peterson, B.J. Schindler, K.L. Killops, M.A. Browe, J.J. Mahle, J. Mater. Chem. A, 1 (2013) 11922.
- [116] P. Pachfule, X. Yang, Q.-L. Zhu, N. Tsumori, T. Uchida, Q. Xu, J. Mater. Chem. A, 5 (2017) 4835-4841.
- [117] J. Qiu, X. Zhang, Y. Feng, X. Zhang, H. Wang, J. Yao, Appl. Catal. B-Environ., 231 (2018) 317-342.
- [118] J. Aguilera-Sigalat, D. Bradshaw, Coord. Chem. Rev., 307 (2016) 267-291.
- [119] X.-B. Meng, J.-L. Sheng, H.-L. Tang, X.-J. Sun, H. Dong, F.-M. Zhang, Appl. Catal. B-Environ., 244 (2019) 340-346.
- [120] Q. Wang, G. Wang, X. Liang, X. Dong, X. Zhang, Appl. Surf. Sci., 467-468 (2019) 320-327.
- [121] D. Esken, H. Noei, Y. Wang, C. Wiktor, S. Turner, G. Van Tendeloo, R.A. Fischer, J. Mater. Chem., 21 (2011) 5907.
- [122] D. Esken, S. Turner, C. Wiktor, S.B. Kalidindi, G. Van Tendeloo, R.A. Fischer, JACS, 133 (2011) 16370-16373.
- [123] Y. Gao, J. Wu, W. Zhang, Y. Tan, J. Zhao, B. Tang, Mater. Lett., 128 (2014) 208-211.
- [124] Z. Chen, Z.-G. Gu, W.-Q. Fu, F. Wang, J. Zhang, ACS Appl. Mater. Interfaces, 8 (2016) 28737-28742.
- [125] D. Zhang, J. Zhao, Q. Liu, Z. Xia, Inorg. Chem., 58 (2019) 1690-1696.
- [126] Q. Yang, Y.Z. Chen, Z.U. Wang, Q. Xu, H.L. Jiang, Chem. Commun., 51 (2015) 10419-10422.
- [127] R. Kaur, A.L. Sharma, K.-H. Kim, A. Deep, J. Ind. Eng. Chem., 53 (2017) 77-81.
- [128] L. Chen, H. Chen, R. Luque, Y. Li, Chem. Sci., 5 (2014) 3708-3714.
- [129] R. Lin, L. Shen, Z. Ren, W. Wu, Y. Tan, H. Fu, J. Zhang, L. Wu, Chem. Commun., 50 (2014) 8533-8535.
- [130] H. Wang, X. Yuan, Y. Wu, X. Chen, L. Leng, G. Zeng, RSC Adv., 5 (2015) 32531-32535.
- [131] S. Jin, H.-J. Son, O.K. Farha, G.P. Wiederrecht, J.T. Hupp, JACS, 135 (2013) 955-958.
- [132] J. Huang, H. Song, C. Chen, Y. Yang, N. Xu, X. Ji, C. Li, J.-A. You, J. Environ. Chem. Eng., 5 (2017) 2579-2585.
- [133] H. Sammi, D. Kukkar, J. Singh, P. Kukkar, R. Kaur, H. Kaur, M. Rawat, G. Singh, K.-H. Kim, Sens. Actuators, B, 255 (2018) 3047-3056.
- [134] J. Ren, T. Li, X. Zhou, X. Dong, A.V. Shorokhov, M.B. Semenov, V.D. Krevchik, Y. Wang, Chem. Eng. J., 358 (2019) 30-39.
- [135] Z. Huang, H. Chen, L. Zhao, X. He, W. Fang, Y. Du, W. Li, G. Wang, F. Zhang, J. Mater. Sci.-Mater. Electron., 29 (2018) 12045-12054.
- [136] W.-L. Xin, L.-F. Jiang, L.-P. Zong, H.-B. Zeng, G.-F. Shu, R. Marks, X.-J. Zhang, D. Shan, Sens. Actuators, B, 273 (2018) 566-573.
- [137] S. Wan, M. Ou, Q. Zhong, X. Wang, Chem. Eng. J., 358 (2019) 1287-1295.
- [138] Z. Li, F. Bu, J. Wei, W. Yao, L. Wang, Z. Chen, D. Pan, M. Wu, Nanoscale, 10 (2018) 22871-22883.
- [139] Z. Li, X. Liu, L. Wang, F. Bu, J. Wei, D. Pan, M. Wu, Small, 14 (2018).
- [140] R. Lin, S. Li, J. Wang, J. Xu, C. Xu, J. Wang, C. Li, Z. Li, Inorg. Chem. Front., 5 (2018) 3170-3177.
- [141] X. Hao, Z. Jin, H. Yang, G. Lu, Y. Bi, Appl. Catal. B-Environ., 210 (2017) 45-56.
- [142] F. Sun, Q. Li, H. Xue, H. Pang, Chemelectrochem, 6 (2019) 1273-1299.
- [143] A. Fujishima, K. Honda, Nature, 238 (1972) 37-38.
- [144] X.B. Fan, S. Yu, B. Hou, J.M. Kim, Isr. J. Chem., 59 (2019) 762-773.

- [145] Q. Xu, B. Zhu, B. Cheng, J. Yu, M. Zhou, W. Ho, *Appl. Catal. B-Environ.*, 255 (2019).
- [146] S. Saha, G. Das, J. Thote, R. Banerjee, *JACS*, 136 (2014) 14845-14851.
- [147] P.P. Bag, X.-S. Wang, P. Sahoo, J. Xiong, R. Cao, *Catal. Sci. Technol.*, 7 (2017) 5113-5119.
- [148] J.B. Sambur, T.-Y. Chen, E. Choudhary, G. Chen, E.J. Nissen, E.M. Thomas, N. Zou, P. Chen, *Nature*, 530 (2016) 77-+.
- [149] S.R. Vaddipalli, S.R. Sanivarapu, S. Vengatesan, J.B. Lawrence, M. Eashwar, G. Sreedhar, *ACS Appl. Mater. Interfaces*, 8 (2016) 23049-23059.
- [150] X. Li, J.G. Yu, J.X. Low, Y.P. Fang, J. Xiao, X.B. Chen, *J. Mater. Chem. A*, 3 (2015) 2485-2534.
- [151] S. Kampouri, T.N. Nguyen, M. Spodaryk, R.G. Palgrave, A. Züttel, B. Smit, K.C. Stylianou, *Adv. Funct. Mater.*, 28 (2018).
- [152] D. Sun, Y. Fu, W. Liu, L. Ye, D. Wang, L. Yang, X. Fu, Z. Li, *Chemistry-a European Journal*, 19 (2013) 14279-14285.
- [153] Z.B. Liang, C. Qu, W.H. Guo, R.Q. Zou, Q. Xu, *Adv. Mater.*, 30 (2018).
- [154] C. Liu, B.C. Colon, M. Ziesack, P.A. Silver, D.G. Nocera, *Science*, 352 (2016) 1210-1213.
- [155] W.-G. Cui, G.-Y. Zhang, T.-L. Hu, X.-H. Bu, *Coord. Chem. Rev.*, 387 (2019) 79-120.
- [156] Z. Zhao, J. Ding, R. Zhu, H. Pang, *J. Mater. Chem. A*, 7 (2019) 15519-15540.
- [157] A. Crake, K.C. Christoforidis, A. Gregg, B. Moss, A. Kafizas, C. Petit, *Small*, 15 (2019).
- [158] Z.-C. Kong, J.-F. Liao, Y.-J. Dong, Y.-F. Xu, H.-Y. Chen, D.-B. Kuang, C.-Y. Su, *ACS Energy Lett.*, 3 (2018) 2656-2662.
- [159] C.A. Martinez-Huitle, E. Brillas, *Appl. Catal. B-Environ.*, 87 (2009) 105-145.
- [160] Y. Liu, G. Zeng, H. Zhong, Z. Wang, Z. Liu, M. Cheng, G. Liu, X. Yang, S. Liu, *J. Hazard. Mater.*, 322 (2017) 394-401.
- [161] M. Cheng, G.M. Zeng, D.L. Huang, C. Lai, Y. Liu, C. Zhang, R.Z. Wang, L. Qin, W.J. Xue, B.A. Song, S.J. Ye, H. Yi, *J. Colloid Interface Sci.*, 515 (2018) 232-239.
- [162] C.-C. Wang, J.-R. Li, X.-L. Lv, Y.-Q. Zhang, G. Guo, *Energy Environ. Sci.*, 7 (2014) 2831-2867.
- [163] R. Kaur, K. Vellingiri, K.-H. Kim, A.K. Paul, A. Deep, *Chemosphere*, 154 (2016) 620-627.
- [164] R. Kaur, A. Rana, R.K. Singh, V.A. Chhabra, K.-H. Kim, A. Deep, *RSC Adv.*, 7 (2017) 29015-29024.
- [165] M. Cheng, G. Zeng, D. Huang, C. Lai, Y. Liu, P. Xu, C. Zhang, J. Wan, L. Hu, W. Xiong, C. Zhou, *Chem. Eng. J.*, 327 (2017) 686-693.
- [166] M. Cheng, Y. Liu, D. Huang, C. Lai, G. Zeng, J. Huang, Z. Liu, C. Zhang, C. Zhou, L. Qin, W. Xiong, H. Yi, Y. Yang, *Chem. Eng. J.*, 362 (2019) 865-876.
- [167] Y. Zou, X. Wang, A. Khan, P. Wang, Y. Liu, A. Alsaedi, T. Hayat, X. Wang, *Environ. Sci. Technol.*, 50 (2016) 7290-7304.
- [168] M.A. Barakat, *Arabian J. Chem.*, 4 (2011) 361-377.
- [169] S. Bolisetty, M. Peydayesh, R. Mezzenga, *Chem. Soc. Rev.*, 48 (2019) 463-487.
- [170] C.-C. Wang, X.-D. Du, J. Li, X.-X. Guo, P. Wang, J. Zhang, *Appl. Catal. B-Environ.*, 193 (2016) 198-216.
- [171] M. Feng, P. Zhang, H.-C. Zhou, V.K. Sharma, *Chemosphere*, 209 (2018) 783-800.
- [172] S. Xiao, D. Pan, R. Liang, W. Dai, Q. Zhang, G. Zhang, C. Su, H. Li, W. Chen, *Appl. Catal. B-Environ.*, 236 (2018) 304-313.
- [173] W. Yang, X. Li, Y. Li, R. Zhu, H. Pang, *Adv. Mater.*, 31 (2019).
- [174] J. Li, W. Zhang, M. Ran, Y. Sun, H. Huang, F. Dong, *Appl. Catal. B-Environ.*, 243 (2019) 313-321.
- [175] S. Gao, W. Cen, Q. Li, J. Li, Y. Lu, H. Wang, Z. Wu, *Appl. Catal. B-Environ.*, 227 (2018) 190-197.
- [176] B. Wang, Z. Deng, X. Fu, Z. Li, *J. Mater. Chem. A*, 6 (2018) 19735-19742.

- [177] Y. Lu, X. Cheng, G. Tian, H. Zhao, L. He, J. Hu, S.-M. Wu, Y. Dong, G.-G. Chang, S. Lenaerts, S. Siffert, G. Van Tendeloo, Z.-F. Li, L.-L. Xu, X.-Y. Yang, B.-L. Su, *Nano Energy*, 47 (2018) 8-17.
- [178] J. Zhang, Y. Huang, Y. Dan, L. Jiang, *Appl. Surf. Sci.*, 488 (2019) 228-236.
- [179] L. Zhang, Z. Xi, M. Xing, J. Zhang, *Int. J. Hydrogen Energy*, 38 (2013) 9169-9177.
- [180] T. Hisatomi, K. Takahabe, K. Domen, *Catal. Lett.*, 145 (2014) 95-108.
- [181] P. Zhou, J. Yu, M. Jaroniec, *Adv. Mater.*, 26 (2014) 4920-4935.

Table 1 The application of QD-MOF composites in photocatalytic energy generation and environmental remediation.

QD	MOF	Application	Synthesis method	Efficiency	Reference
CdS	MIL-101/MOF-5	Hydrogen production	Ship-in-a-bottle	75.5/0 mmol g ⁻¹ h ⁻¹	[1]
CdS	ZAVCl	Hydrogen production	Bottle-around-the-ship	41.80 mmol g ⁻¹ h ⁻¹	[2]
CdS, CD	MIL-101	Hydrogen production	Ship-in-a-bottle	0.49 mmol g ⁻¹ h ⁻¹	[3]
CdS	UIO-66	Hydrogen production	Photodeposition	13.80 mmol g ⁻¹ h ⁻¹	[4]
CdS	NU-1000	Hydrogen production	Photodeposition	2.42 mmol g ⁻¹ h ⁻¹	[5]
MoS ₂	UIO-66-NH ₂	Hydrogen production	Direct deposition	2.07 mmol g ⁻¹ h ⁻¹	[6]
CdSe	LaBTC	Hydrogen production	Direct surface functionalization	3.20 mmol·(cm ²) ⁻¹	[7]
TiO ₂	Cu ₃ (BTC) ₂	Carbon dioxide reduction	Physical mixing	2.64 μmol g ⁻¹ h ⁻¹	[8]
CsPbBr ₃	ZIF-8/ZIF-67	Carbon dioxide reduction	Bottle-around-the-ship	1.50/3.51 μmol g ⁻¹ h ⁻¹	[9]
CsPbBr ₃	UIO-66(NH ₂)	Carbon dioxide reduction	Direct surface functionalization	0.26 μmol g ⁻¹ h ⁻¹	[10]
CdTe	Eu-MOF	Dye degradation (Rh 6G)	Direct surface functionalization	>98.00%	[11]
CdTe	NTU-9	Dye degradation (Rh 6G)	Bottle-around-the-ship	>95.00%	[12]
CdSe	UIO-66	Dye degradation (RhB)	Ship-in-a-bottle	100.00%	[13]
CdSe	MIL-125	Dye degradation (RhB)	Physical mixing	>98.00%	[14]
CQD	NH ₂ -MIL-125	Dye degradation (RhB)	Ship-in-a-bottle	100.00%	[15]
N-TiO ₂	MIL-100(Fe)	Dye degradation (MB/RhB)	Physical mixing	99.10%/93.50%	[16]
Ag ₂ S/CdS/CuS	MIL-125 (Ti)	Cr (VI) reduction	Photochemical deposition	77.50%/65.00%/47.50%	[17]
CQD	MIL-53(Fe)	Cr(VI) reduction	Ship-in-a-bottle	85.00%	[18]
CdS	NH ₂ -MIL-125	Nitric oxide oxidation	Ship-in-a-bottle	48.40%	[19]

[1] J. He, Z. Yan, J. Wang, J. Xie, L. Jiang, Y. Shi, F. Yuan, F. Yu, Y. Sun, Chem. Commun., 49 (2013) 6761-6763.

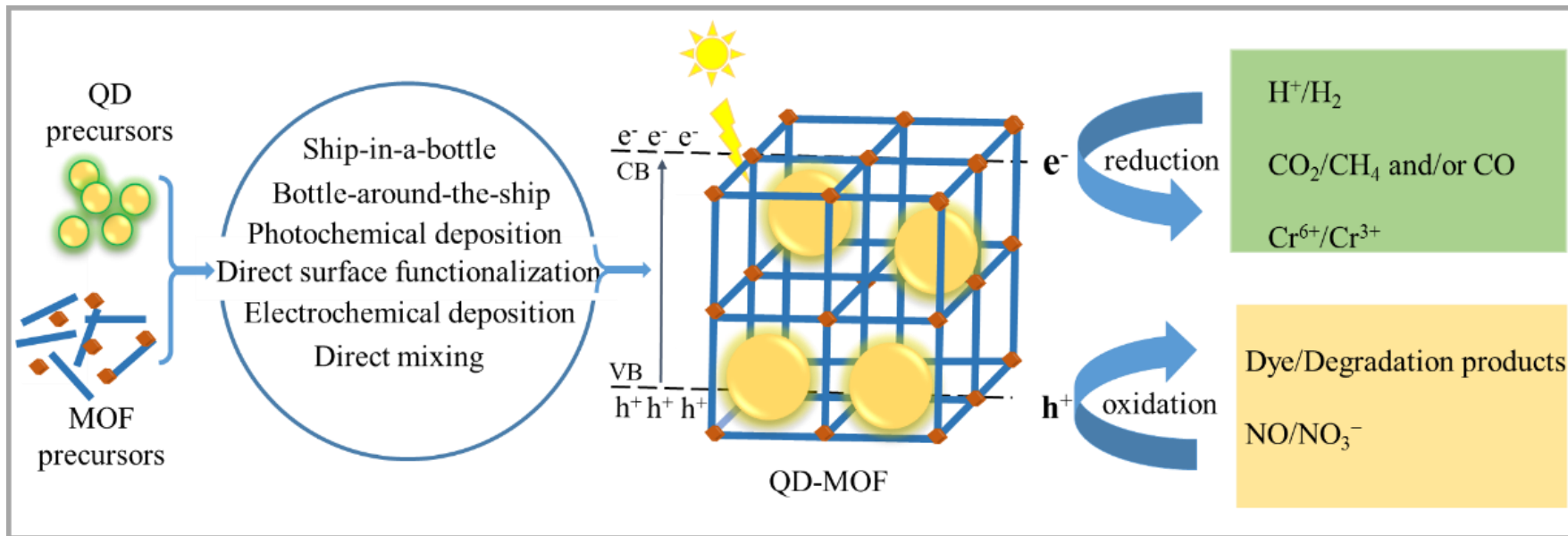
[2] S. Saha, G. Das, J. Thote, R. Banerjee, JACS, 136 (2014) 14845-14851.

[3] X.-B. Meng, J.-L. Sheng, H.-L. Tang, X.-J. Sun, H. Dong, F.-M. Zhang, Appl. Catal. B-Environ., 244 (2019) 340-346.

[4] R. Lin, L. Shen, Z. Ren, W. Wu, Y. Tan, H. Fu, J. Zhang, L. Wu, Chem. Commun., 50 (2014) 8533-8535.

- [5] P.P. Bag, X.-S. Wang, P. Sahoo, J. Xiong, R. Cao, *Catal. Sci. Technol.*, 7 (2017) 5113-5119.
- [6] X. Hao, Z. Jin, H. Yang, G. Lu, Y. Bi, *Appl. Catal. B-Environ.*, 210 (2017) 45-56.
- [7] S.R. Vaddipalli, S.R. Sanivarapu, S. Vengatesan, J.B. Lawrence, M. Eashwar, G. Sreedhar, *ACS Appl. Mater. Interfaces*, 8 (2016) 23049-23059.
- [8] R. Li, J.H. Hu, M.S. Deng, H.L. Wang, X.J. Wang, Y.L. Hu, H.L. Jiang, J. Jiang, Q. Zhang, Y. Xie, Y.J. Xiong, *Adv. Mater.*, 26 (2014) 4783-+.
- [9] Z.-C. Kong, J.-F. Liao, Y.-J. Dong, Y.-F. Xu, H.-Y. Chen, D.-B. Kuang, C.-Y. Su, *ACS Energy Lett.*, 3 (2018) 2656-2662.
- [10] S. Wan, M. Ou, Q. Zhong, X. Wang, *Chem. Eng. J.*, 358 (2019) 1287-1295.
- [11] R. Kaur, K. Vellingiri, K.-H. Kim, A.K. Paul, A. Deep, *Chemosphere*, 154 (2016) 620-627.
- [12] R. Kaur, A. Rana, R.K. Singh, V.A. Chhabra, K.-H. Kim, A. Deep, *Rsc Advances*, 7 (2017) 29015-29024.
- [13] H. Gan, Z. Wang, H. Li, Y. Wang, L. Sun, Y. Li, *RSC Adv.*, 6 (2016) 5192-5197.
- [14] Z. Huang, H. Chen, L. Zhao, X. He, W. Fang, Y. Du, W. Li, G. Wang, F. Zhang, *J. Mater. Sci. - Mater. Electron.*, 29 (2018) 12045-12054.
- [15] Q. Wang, G. Wang, X. Liang, X. Dong, X. Zhang, *Appl. Surf. Sci.*, 467-468 (2019) 320-327.
- [16] J. Huang, H. Song, C. Chen, Y. Yang, N. Xu, X. Ji, C. Li, J.-A. You, *J. Environ. Chem. Eng.*, 5 (2017) 2579-2585.
- [17] H. Wang, X. Yuan, Y. Wu, X. Chen, L. Leng, G. Zeng, *RSC Adv.*, 5 (2015) 32531-32535.
- [18] R. Lin, S. Li, J. Wang, J. Xu, C. Xu, J. Wang, C. Li, Z. Li, *Inorg. Chem. Front.*, 5 (2018) 3170-3177.
- [19] S. Gao, W. Cen, Q. Li, J. Li, Y. Lu, H. Wang, Z. Wu, *Appl. Catal. B-Environ.*, 227 (2018) 190-197.

Graphical abstract



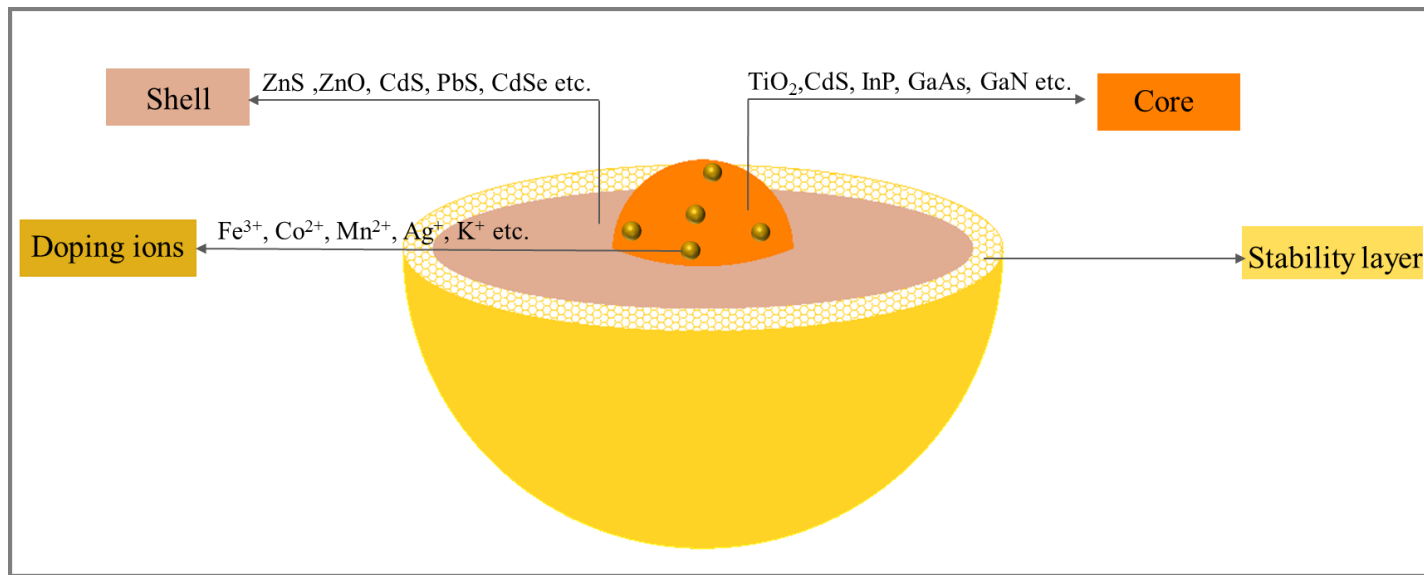


Fig. 1 The structure of QDs.

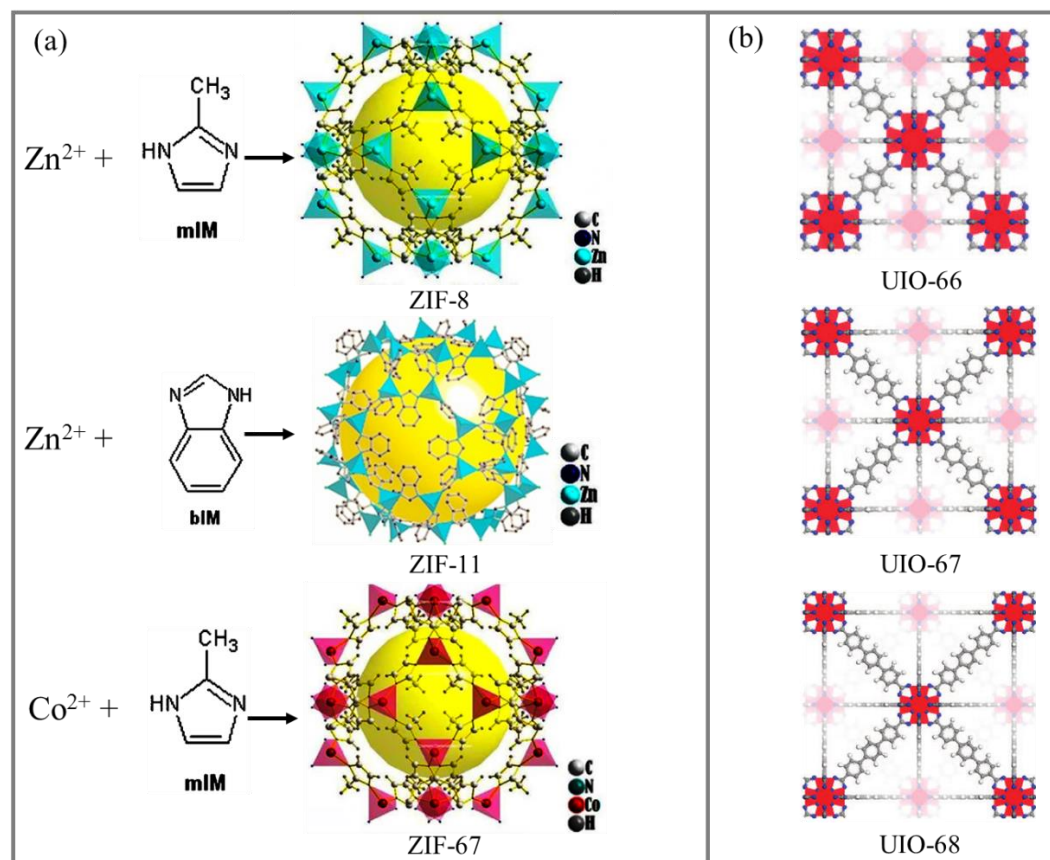
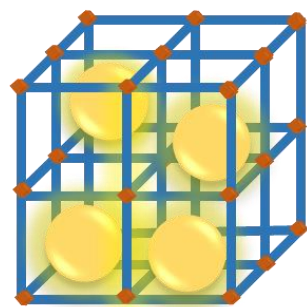
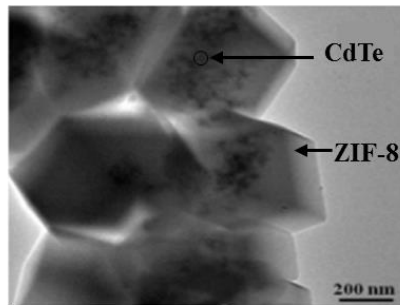


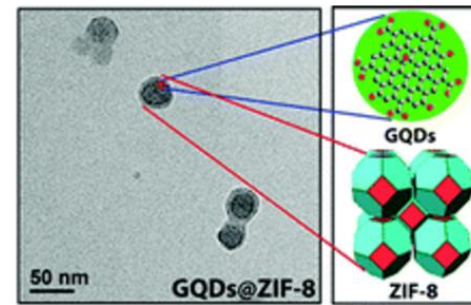
Fig. 2 (a) The structures of ZIF-8, ZIF-11 and ZIF-67. Reproduced with permission from ref. [1, 2]. Copyright 2006 Elsevier and 2010 American Chemical Society. (b) The structures of UIO-66, UIO-67 and UIO-68. Reproduced with permission from ref. [3]. Copyright 2008 American Chemical Society.



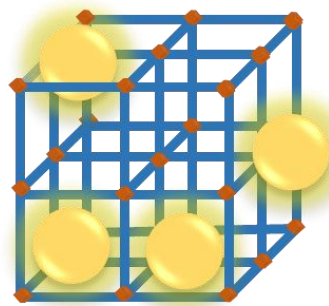
(a)



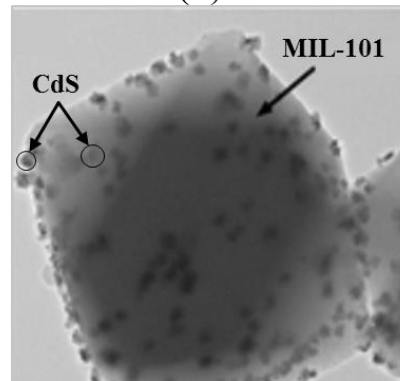
(b)



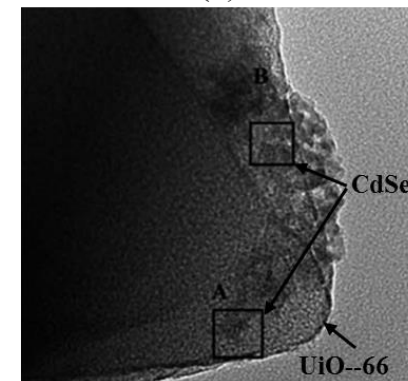
(c)



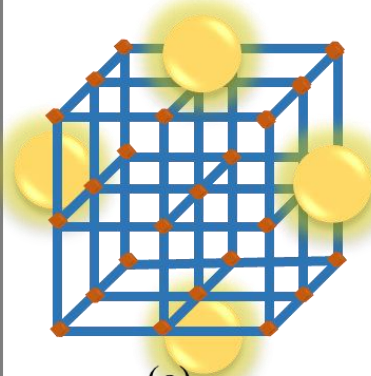
(d)



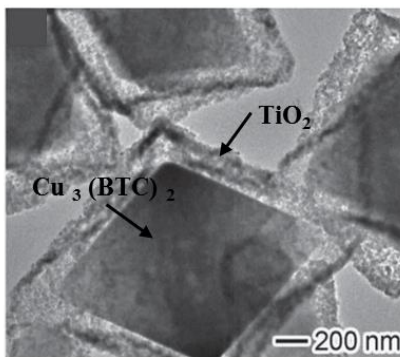
(e)



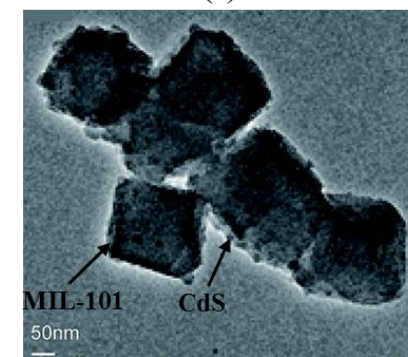
(f)



(g)



(h)



(i)

Fig. 3 Three structures of QD-MOF composites. (a) The model of “QDs are almost encapsulated within the MOF matrix”; (b) CdTe QDs were encapsulated in ZIF-8. Reproduced with permission from ref. [4]. Copyright 2017 Elsevier. (c) GQDs were encapsulated in ZIF-8. Reproduced with permission from ref. [5]. Copyright 2013 The Royal Society of Chemistry. (d) The model of “QDs exist both inside and outside of the MOF matrix”. (e) The CdS QDs were embedded into MIL-101 and excessive QDs were agglomerated on the MIL-101 surface. Reproduced with permission from ref. [6]. Copyright 2013 The Royal Society of Chemistry. (f) CdSe QDs were grew both inside and outside of the UiO-66. Reproduced with permission from ref. [7]. Copyright 2016 The Royal Society of Chemistry. (g) The model of “QDs are almost deposited on the outer surface of the MOF matrix”. (h) TiO₂ QDs were deposited on the surface of MIL-101. Reproduced with permission from ref. [8]. Copyright 2014 WILEY-VCH. (i) ZnO QDs were deposited on the surface of ZUM. Reproduced with permission from ref. [9]. Copyright 2017 The Royal Society of Chemistry.

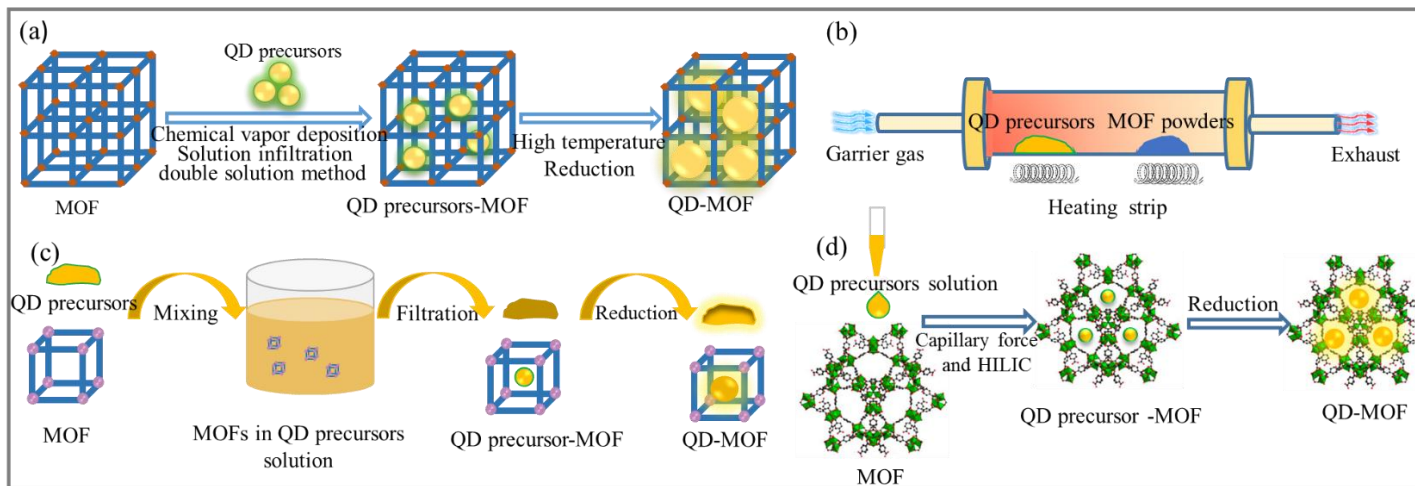


Fig. 4 The schematic diagram of “ship-in-a-bottle”: (a) Universal schematic diagram of “ship-in-a-bottle”; (b) Chemical vapor deposition; (c) Solution infiltration; (d) Double solution method. (b) and (c) are adapted with permission from ref [10]. Copyright 2017 Elsevier.

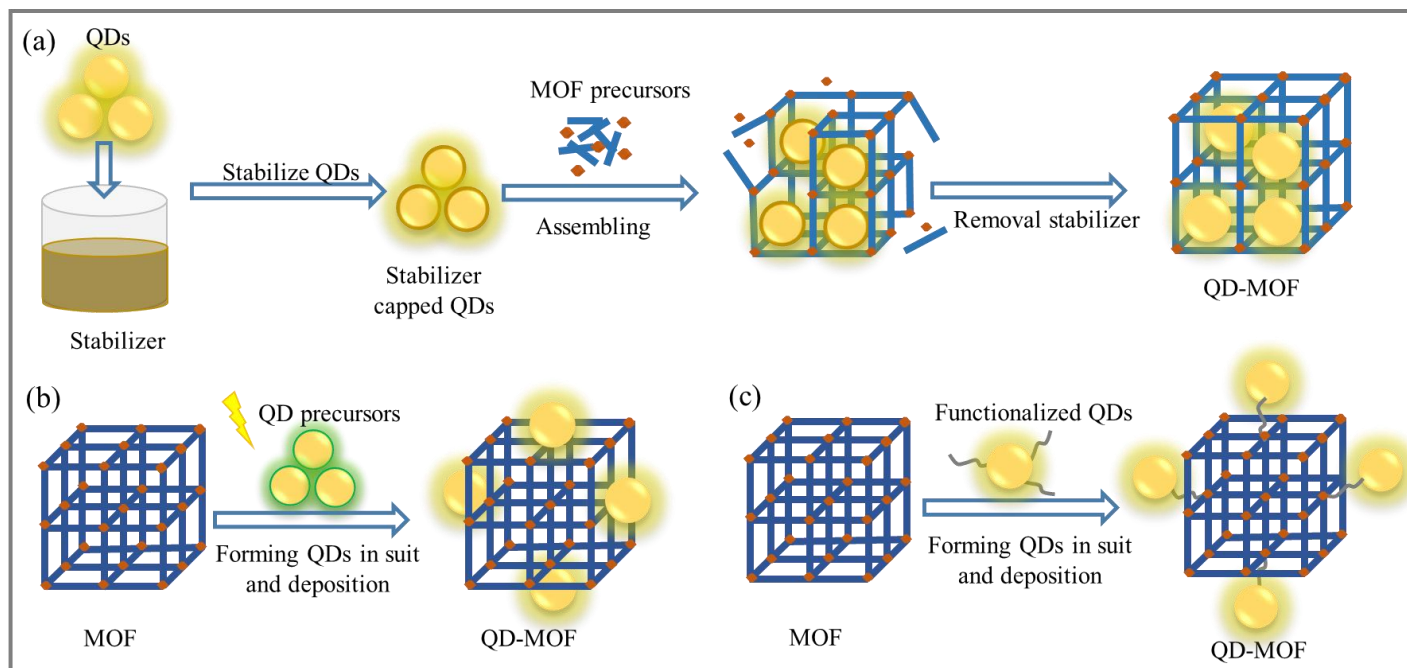


Fig. 5 (a) The method of “bottle-around-the-ship”. (b) The method of “photochemical deposition”. (c) The method of “direct surface functionalization”. (b) and (c) are adapted with permission from ref [11]. Copyright 2016 Elsevier.

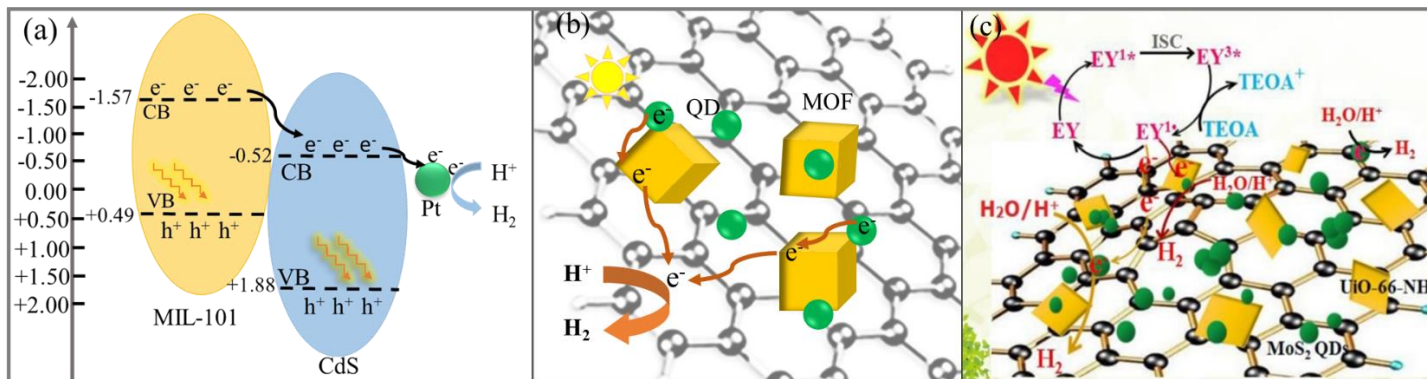


Fig. 6 (a) The photocatalytic hydrogen evolution mechanism of CdS/MIL-101. (b) The photocatalytic hydrogen evolution mechanism of UIO-66/CdS/RGO or CdS@NU-1000/RGO. (c) The photocatalytic hydrogen evolution mechanism of EY sensitized MoS₂ QDs/UiO-66-NH₂/G.

Reproduced with permission from ref. [12]. Copyright 2017 Elsevier.



Fig. 7 (a) The schematic diagram of photoelectrode transformation from Au NPs/CdSe/LaBTC to Au NPs/CdS/LaBTC and the electron transport path of them. (b) The band energy diagram and electron transfer mechanism of Au NPs-CdSe QDs sensitized LaBTC MOFs. Reproduced with permission from ref. [13]. Copyright 2016 American Chemical Society.

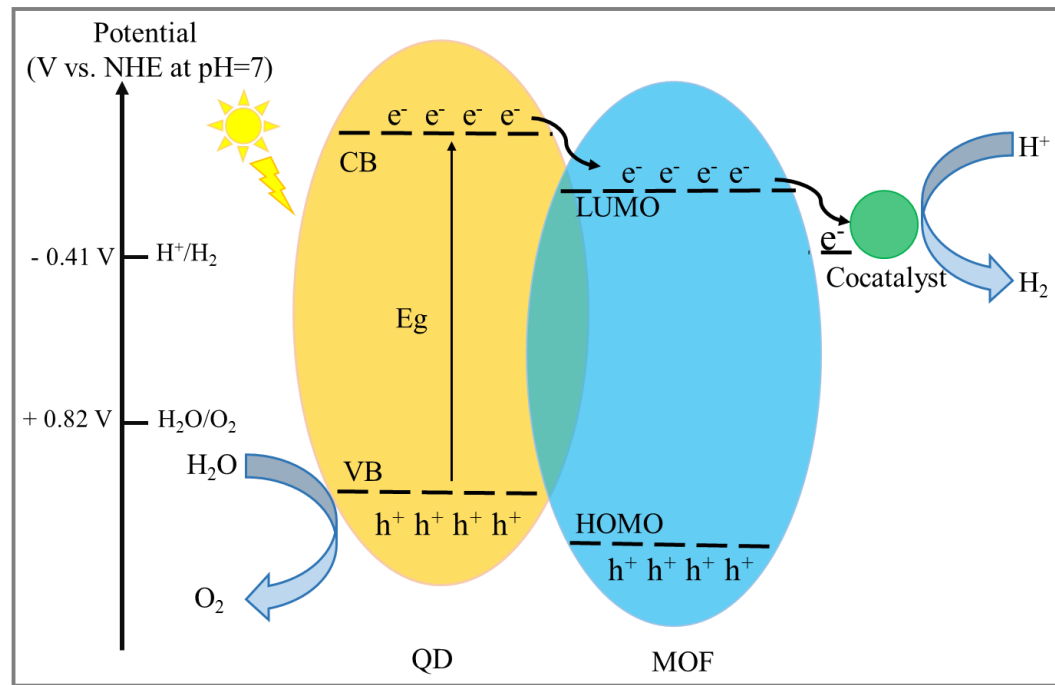


Fig. 8 The general mechanism of photocatalytic water splitting by QD-MOF composites.

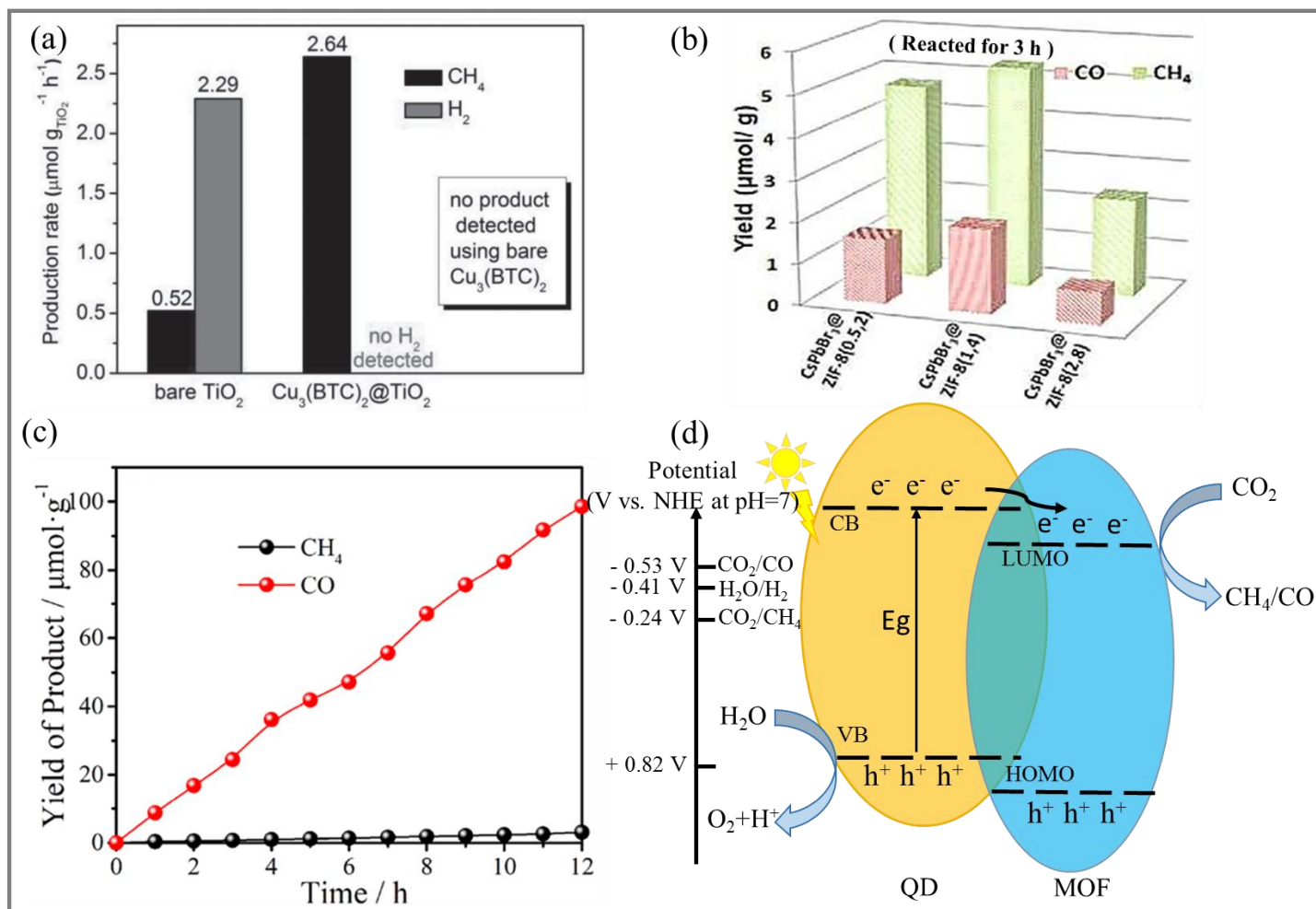


Fig. 9 (a) The production rate of CH₄ and H₂ from CO₂ by using Cu₃ (BTC)₂ @TiO₂. Reproduced with permission from ref.[8]. Copyright. 2014

WILEY-VCH. (b) The yield of CH₄ and CO after 3 h by using CsPbBr₃ and CsPbBr₃@ZIFs. Reproduced with permission from ref. [14].
Copyright 2018 American Chemical Society. (c) The yield of CH₄ and CO by using 15%-CsPbBr₃ QDs UiO-66(NH₂). Reproduced with
permission from ref. [15]. Copyright 2109 Elsevier. (d) The photocatalytic mechanism of CO₂ reduction by QD-MOF composites.

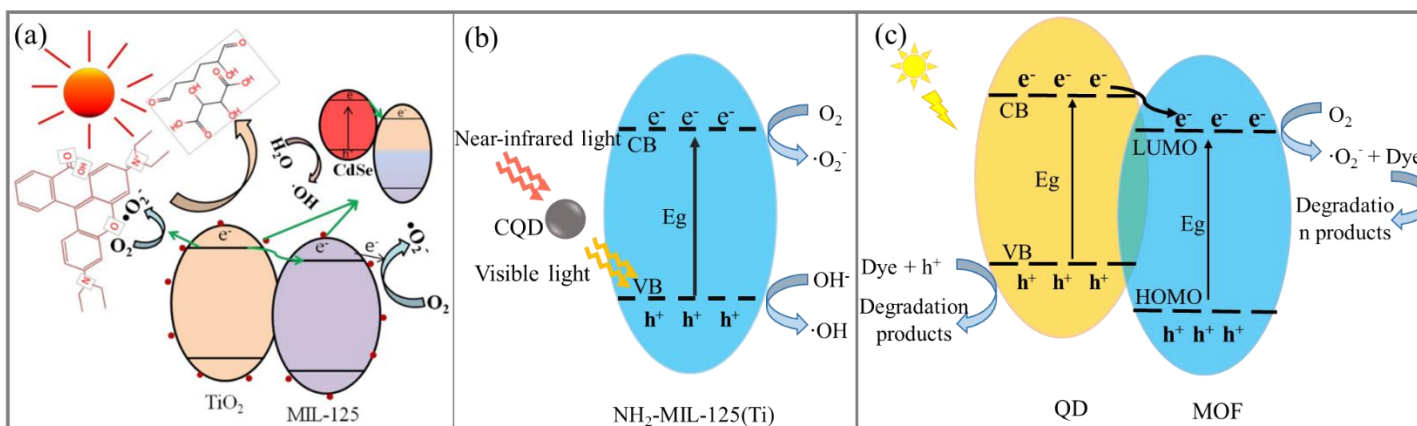


Fig. 10 (a) The energy band position and photocatalytic mechanism of MIL-125(Ti)/TiO₂@SiO₂ two-level type-II heterostructure. Reproduced with permission from ref. [16]. Copyright 2018 Springer. (b) The schematic diagram of CQD upconversion and photocatalytic mechanism of CQD/NH₂-MIL-125(Ti). (c) The mechanism of photocatalytic degradation of dyes by QD-MOF composites.

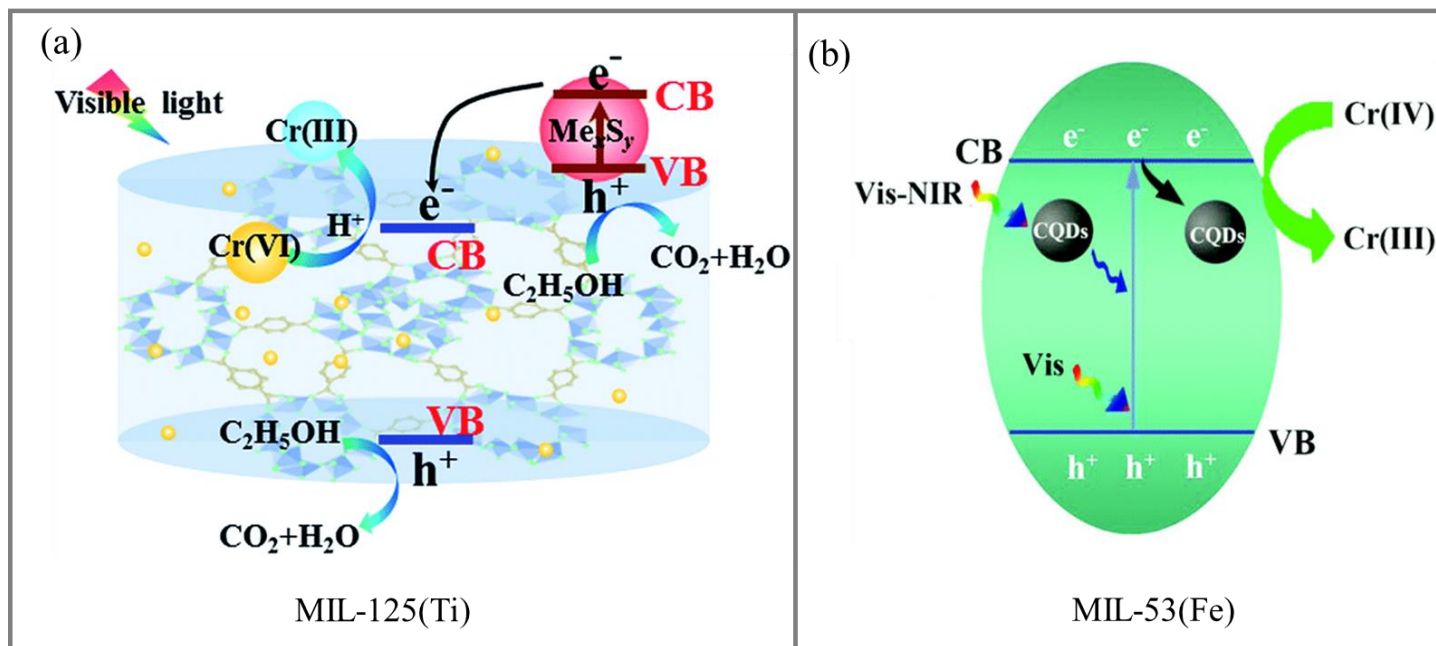


Fig. 11 (a) The photocatalytic reduction mechanism of Cr (VI) by metallic sulfide (Ag₂S, CdS and CuS QDs) modified MIL-125 (Ti). Reproduced with permission from ref. [17]. Copyright 2015 The Royal Society of Chemistry. (b) Cr (VI) by MIL-53 (Fe)/CQD. Reproduced with permission from ref. [18]. Copyright 2108 Partner Organisations.

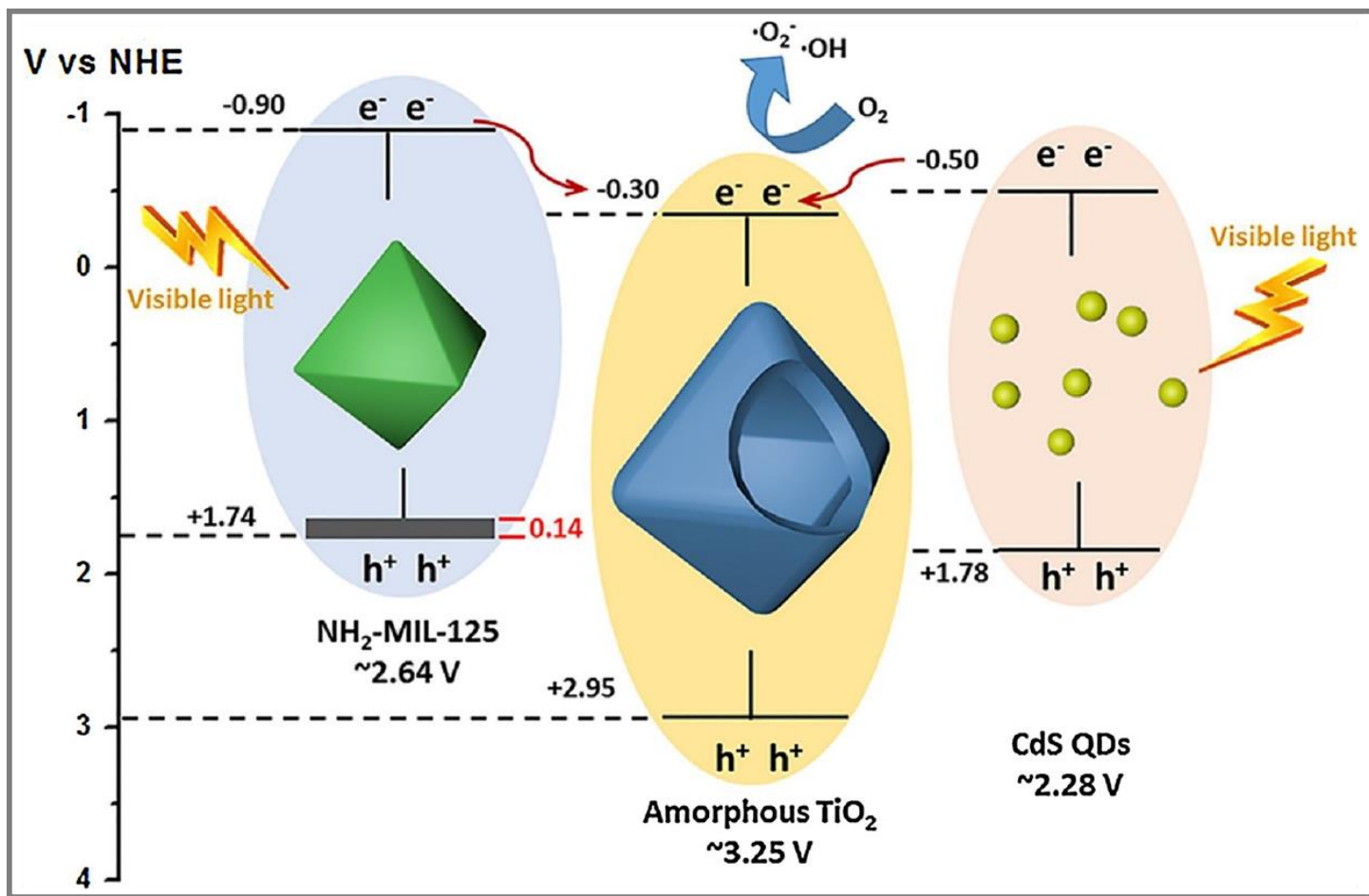


Fig. 12 The mechanism of photocatalytic oxidation of NO over CdS QDs/NH₂-MIL-125@TiO₂. Reproduced with permission from ref. [19].

Copyright 2018 Elsevier.

- [1] K.S. Park, Z. Ni, A.P. Cote, J.Y. Choi, R. Huang, F.J. Uribe-Romo, H.K. Chae, M. O'Keeffe, O.M. Yaghi, *Proc Natl Acad Sci U S A*, 103 (2006) 10186-10191.
- [2] B. Assfour, S. Leoni, G. Seifert, *J. Phys. Chem. C*, 114 (2010) 13381-13384.
- [3] J.H. Cavka, S. Jakobsen, U. Olsbye, N. Guillou, C. Lamberti, S. Bordiga, K.P. Lillerud, *JACS*, 130 (2008) 13850-13851.
- [4] K. Wang, N. Li, J. Zhang, Z. Zhang, F. Dang, *Biosens. Bioelectron.*, 87 (2017) 339-344.
- [5] B.P. Biswal, D.B. Shinde, V.K. Pillai, R. Banerjee, *Nanoscale*, 5 (2013) 10556-10561.
- [6] J. He, Z. Yan, J. Wang, J. Xie, L. Jiang, Y. Shi, F. Yuan, F. Yu, Y. Sun, *Chem. Commun.*, 49 (2013) 6761-6763.
- [7] H. Gan, Z. Wang, H. Li, Y. Wang, L. Sun, Y. Li, *RSC Adv.*, 6 (2016) 5192-5197.
- [8] R. Li, J.H. Hu, M.S. Deng, H.L. Wang, X.J. Wang, Y.L. Hu, H.L. Jiang, J. Jiang, Q. Zhang, Y. Xie, Y.J. Xiong, *Adv. Mater.*, 26 (2014) 4783-+.
- [9] X.-Y. Xu, B. Yan, *J. Mater. Chem. A*, 5 (2017) 2215-2223.
- [10] P. Railey, Y. Song, T. Liu, Y. Li, *Mater. Res. Bull.*, 96 (2017) 385-394.
- [11] J. Aguilera-Sigalat, D. Bradshaw, *Coord. Chem. Rev.*, 307 (2016) 267-291.
- [12] X. Hao, Z. Jin, H. Yang, G. Lu, Y. Bi, *Appl. Catal. B-Environ*, 210 (2017) 45-56.
- [13] S.R. Vaddipalli, S.R. Sanivarapu, S. Vengatesan, J.B. Lawrence, M. Eashwar, G. Sreedhar, *ACS Appl. Mater. Interfaces*, 8 (2016) 23049-23059.
- [14] Z.-C. Kong, J.-F. Liao, Y.-J. Dong, Y.-F. Xu, H.-Y. Chen, D.-B. Kuang, C.-Y. Su, *ACS Energy Lett.*, 3 (2018) 2656-2662.
- [15] S. Wan, M. Ou, Q. Zhong, X. Wang, *Chem. Eng. J.*, 358 (2019) 1287-1295.
- [16] Z. Huang, H. Chen, L. Zhao, X. He, W. Fang, Y. Du, W. Li, G. Wang, F. Zhang, *J. Mater. Sci.-Mater. Electron.*, 29 (2018) 12045-12054.
- [17] H. Wang, X. Yuan, Y. Wu, X. Chen, L. Leng, G. Zeng, *RSC Adv.*, 5 (2015) 32531-32535.
- [18] R. Lin, S. Li, J. Wang, J. Xu, C. Xu, J. Wang, C. Li, Z. Li, *Inorg. Chem. Front.*, 5 (2018) 3170-3177.
- [19] S. Gao, W. Cen, Q. Li, J. Li, Y. Lu, H. Wang, Z. Wu, *Appl. Catal. B-Environ.*, 227 (2018) 190-197.